

# Various features of quasiequilibrium sequences of binary neutron stars in general relativity

Keisuke Taniguchi\*

*Department of Earth Science and Astronomy, Graduate School of Arts and Sciences,  
University of Tokyo, Komaba, Meguro, Tokyo 153-8902, Japan*

Ericourgoulhon†

*Laboratoire de l'Univers et de ses Théories, UMR 8102 du C.N.R.S.,  
Observatoire de Paris, F-92195 Meudon Cedex, France*

(Dated: 25 August 2003)

Quasiequilibrium sequences of binary neutron stars are numerically calculated in the framework of the Isenberg-Wilson-Mathews (IWM) approximation of general relativity. The results are presented for both rotation states of synchronized spins and irrotational motion, while the latter is considered as the realistic one for binary neutron stars just prior to merger. We assume a polytropic equation of state and compute several evolutionary sequences of binary systems composed of different-mass stars as well as identical-mass stars with adiabatic indices  $\gamma = 2.5, 2.25, 2,$  and  $1.8$ . From our results, we propose as a conjecture that if the turning point of binding energy (and total angular momentum) locating the innermost stable circular orbit (ISCO) is found in the Newtonian gravity for some value of the adiabatic index  $\gamma_0$ , that of the ADM mass (and total angular momentum) should exist in the IWM approximation of general relativity for the same value of the adiabatic index.

PACS numbers: 04.25.Dm, 04.40.Dg, 97.60.Jd, 97.80.-d

## I. INTRODUCTION

The final stage of coalescing binary neutron stars is one of the most promising sources of gravitational waves for ground-based laser interferometers such as GEO600, LIGO, TAMA300, and VIRGO [1]. It is also considered as one of the candidates for short-duration gamma-ray burst sources [2]. If we have accurate templates of gravitational waves from coalescing binary neutron stars, it may be possible to extract informations from signals observed by the above interferometers [3], through the matched filtering technique [4]. Therefore, it is essential to theoretically predict the wave form of gravitational radiation as well as to understand the details of the physics of binary neutron stars. With such a motivation, many efforts have been invested in this topic (some reviews can be found in [5, 6]) When summarizing these researches, it is convenient to separate the evolution of binary neutron stars into three phases. The first phase is the *pointlike inspiral* in which the separation between the two stars is much larger than the radius of a star, and the binary system evolves adiabatically. In this stage, the post-Newtonian expansion works excellently, and the accurate wave form of gravitational radiation have been calculated [6, 7, 8]. The second phase is the *intermediate* one or *hydrodynamical inspiral* in which the separation between the two components is as close as a few times of the radius of a star. This phase is also inspiraling, the time scale of the orbital shrink being still larger than the orbital period, hence the qualifier of *quasiequilibrium*. What differs this phase from the pointlike inspiral is that the tidal deformation of the stars is no longer negligible, making necessary a hydrodynamical treatment, in addition to general relativity. The final phase is the *merger*, in which the binary system coalesces dynamically. The first successful merger computations have been obtained by Shibata et al. four years ago [9, 10, 11], and some groups are developing currently [12, 13, 14, 15].

In the present paper, we focus on the intermediate phase (hydrodynamical inspiral). This phase is interesting because we might get informations on the equation of state of nuclear matter [16]. Furthermore, the initial data for computing the merging phase are given at the end point of sequences in the intermediate phase [11]<sup>1</sup>.

---

\*keisuke@providence.c.u-tokyo.ac.jp

†Eric.Gourgoulhon@obspm.fr

<sup>1</sup> Miller and Suen pointed out that the circular orbit condition as an initial data is not a good approximation for corotating neutron star binary systems [17, 18]. As we will describe below, the realistic rotation state of binary neutron stars prior to merger is irrotational flow, and such initial data have been used in Refs. [10, 11]. Furthermore, in Ref. [11], initial data are given at some separations slightly far from the innermost stable circular orbit. We hope that it does not so deviate from the realistic inspiral for irrotational binary neutron stars.

Various approaches to compute binary neutron stars in the intermediate phase have been considered: (1) (semi-)analytical [19, 20] and (2) numerical [21, 22, 23, 24, 25] in the Newtonian gravity, (3) (semi-)analytical [26, 27, 28, 29] and (4) numerical [30] in the post-Newtonian approximation, and (5) numerical in the framework of general relativity [31, 32, 33, 34, 35, 36, 37, 38, 39, 40]. The realistic binary neutron stars gradually decrease their orbital separations driven by the emission of gravitational radiation. However, it is still impossible to integrate the Einstein's equations for many orbits in the intermediate phase. Then the quasiequilibrium configurations are calculated instead of time evolution, because, as we mentioned above, the time scale of the orbital shrink is longer than the orbital period, which justifies to regard the state as quasiequilibrium. In order to combine general relativity and quasiequilibrium, we adopt the conformally flat condition for the spatial part of the metric, so called the Isenberg-Wilson-Mathews (IWM) approximation of general relativity [41, 42, 43] (see [44] for a discussion). This treatment postpones one of the goals of the study of the intermediate phase, i.e. the theoretical prediction of the wave form of gravitational radiation<sup>2</sup> Accordingly, we focus on the other motivation, which is to understand the physics of binary neutron stars in the intermediate phase.

To get a quasiequilibrium configuration of binary neutron stars, we have to specify the rotation state of the system. About ten years ago, Kochanek [47] and Bildsten and Cutler [48] concluded that the irrotational flow is much more realistic than the synchronized rotation, because the shear viscosity of nuclear matter is far too low to synchronize the spins of the stars with the orbital motion by the dynamical merging. The formulation for solving quasiequilibrium configurations of binary neutron stars with irrotational flow in general relativity has been proposed by several authors [49, 50, 51, 52]. Recently a numerical scheme for solving quasiequilibrium figures with arbitrary spins has been introduced by Marronetti and Shapiro [40]. In the present work, we have calculated not only the case of irrotational state but also that of synchronized one in order to compare the differences between these two states. Beside the rotation state, some equation of state for the neutron star matter must be specified to get a binary model. Although the realistic equation of state which is computed by nuclear physicists (see e.g. [53]) has to be used, we adopt here the polytropic one for simplicity. However we vary the polytropic index to cover the large range of nuclear physics equations of state published in the literature. Quasiequilibrium sequences of binary neutron stars based on a selection of realistic equation of state will be presented in a future work.

Under the above assumptions, we have computed quasiequilibrium sequences of binary neutron stars composed of different-mass stars. The observational results of binary pulsars which have neutron star companions such as B1913+16 discovered by Hulse and Taylor [54] show that each star in the binary system has almost the same but slightly different mass<sup>3</sup>. Until now, all studies on quasiequilibrium sequences of binary neutron stars in the framework of general relativity have concerned only identical-mass binary systems except for our previous work [35] (hereafter Paper III). In Paper III, we have obtained quasiequilibrium sequences of binary neutron stars with polytropic equation of state. However, the results have been shown only for the case of adiabatic index  $\gamma = 2$ , because it was the first step to the different-mass binary systems in the framework of general relativity. Then, in the present article, we enlarge the range of adiabatic index.

The plan of the present paper is as follows: Section II provides a brief summary of the assumptions, basic equations, and numerical methods which we adopt. Some code tests not shown in previous articles of this series are given in Sec. III, and the numerical results are presented in Sec. IV. Section V is devoted to the discussions and we conclude the present paper with a summary in Sec. VI. Through the paper, we use units in which  $c = G = 1$ , where  $c$  is the light speed and  $G$  is the gravitational constant.

## II. METHOD

The details about our method and basic equations have been already given in previous papers of this series (Refs. [34] and [24], hereafter Paper I and II respectively). We refer the interested reader to those papers and simply summarize here the basic assumptions, the basic equations and our numerical method.

---

<sup>2</sup> see however Refs. [45, 46] for the computation of gravitational waves from IWM configurations.

<sup>3</sup> The difference in mass of each star is about 4 % for the binary pulsar B1913+16 [55, 56], less than 0.1 % for B1534+12 [55, 57], and about 1 % for B2127+11C [55]

### A. Assumptions

Firstly, we assume the binary system to be in the *quasiequilibrium* state. This assumption comes from the fact that the time scale of the orbital shrink driven by the emission of gravitational radiation is longer than the orbital period:

$$\frac{t_{\text{GW}}}{P_{\text{orb}}} \simeq 1.1 \left( \frac{d}{6M_{\text{tot}}} \right)^{5/2} \left( \frac{M_{\text{tot}}}{4\mu} \right), \quad (1)$$

where  $t_{\text{GW}}$ ,  $P_{\text{orb}}$ ,  $d$ ,  $M_{\text{tot}}$ , and  $\mu$  denote respectively the time scale of the orbital shrink driven by the emission of gravitational radiation, the orbital period, the separation between two stars in the binary system, the total mass, and the reduced mass. The orbit being circular, the quasiequilibrium assumption translates geometrically into the existence of a helical Killing vector in the spacetime:

$$\mathbf{l} = \frac{\partial}{\partial t} + \Omega \frac{\partial}{\partial \varphi}, \quad (2)$$

where  $\Omega$  is the orbital angular velocity and the vectors  $\partial/\partial t$  and  $\partial/\partial \varphi$  are associated with the time coordinate  $t$  and the azimuthal coordinate  $\varphi$  of an asymptotic inertial observer.

The second assumption is applied to the stress-energy tensor, which we require it to have the *perfect fluid* form:

$$T_{\mu\nu} = (e + p)u_\mu u_\nu + pg_{\mu\nu}, \quad (3)$$

where  $e$  denotes the fluid proper energy density,  $p$  the fluid pressure,  $u_\mu$  the fluid 4-velocity, and  $g_{\mu\nu}$  the spacetime metric.

The third assumption concerns the fluid motion inside each star. We consider both cases of *synchronized* (also called *corotating*) and *irrotational* flow, even though the realistic state is regarded as the irrotational one [47, 48]. This is because we would like to reveal the difference between these two states.

The fourth assumption regards the (zero-temperature) equation of state. We choose a *polytropic* one:

$$p = \kappa n^\gamma, \quad (4)$$

where  $n$  is the fluid baryon number density, and  $\kappa$  and  $\gamma$  are some constants. In the present paper, we consider that the two stars in the binary system have the same  $\kappa$  and  $\gamma$ , even if they have different masses.

Finally, we assume the form of the spatial part of the metric to be conformally flat, which is so called the *Isenberg-Wilson-Mathews (IWM)* approximation [41, 42, 43] (see [44] for a discussion).

In this approximation, the spacetime metric takes the form:

$$ds^2 = -(N^2 - B_i B^i) dt^2 - 2B_i dt dx^i + A^2 f_{ij} dx^i dx^j, \quad (5)$$

$N$  being the lapse function,  $B_i$  the shift vector of co-orbiting coordinates,  $A$  the conformal factor, and  $f_{ij}$  the flat spatial metric. The accuracy of this approximation should be checked. The comparison of the non-conformally flat results with the IWM ones will be performed elsewhere [58].

### B. Partial differential equations to be solved

Under the assumptions listed above, we have derived the basic equations in Paper I. Here we present only some outline of them.

The gravitational field equations have been derived within the 3+1 decomposition of the Einstein's equation [59]. The constraint equations are treated in the so-called conformal thin-sandwich approach (see [5, 60] for a review), which enables to take into account the helical symmetry of spacetime. Using the line element of the form of Eq. (5), the trace of the spatial part of the Einstein equation combined with the Hamiltonian constraint equation result in two equations:

$$\underline{\Delta}\nu = 4\pi A^2(E + S) + A^2 K_{ij} K^{ij} - \bar{\nabla}_i \nu \bar{\nabla}^i \beta, \quad (6)$$

$$\underline{\Delta}\beta = 4\pi A^2 S + \frac{3}{4} A^2 K_{ij} K^{ij} - \frac{1}{2} (\bar{\nabla}_i \nu \bar{\nabla}^i \nu + \bar{\nabla}_i \beta \bar{\nabla}^i \beta), \quad (7)$$

where  $\bar{\nabla}_i$  stands for the covariant derivative associated with the flat 3-metric  $f_{ij}$ . The quantities  $\nu$  and  $\beta$  are defined as  $\nu := \ln N$  and  $\beta := \ln(AN)$ , and  $K_{ij}$  denotes the extrinsic curvature tensor.  $E$  and  $S$  are the matter energy density

and the trace of the stress tensor, respectively, which are defined as

$$E := n^\mu n^\nu T_{\mu\nu}, \quad (8)$$

$$S := \gamma_{ij} T^{ij}. \quad (9)$$

In these equations,  $n^\mu$  is the timelike unit normal vector to the hypersurfaces  $t = \text{const}$  and  $\gamma_{ij}$  the spatial 3-metric. We also solve the momentum constraint equation, which yields

$$\underline{\Delta} N^i + \frac{1}{3} \bar{\nabla}^i (\bar{\nabla}_j N^j) = -16\pi N A^2 (E + p) U^i + 2N A^2 K^{ij} \bar{\nabla}_j (3\beta - 4\nu), \quad (10)$$

where  $N^i := B^i + \Omega(\partial/\partial\varphi)$  denotes the shift vector of nonrotating coordinates. In the equations above,  $\underline{\Delta} := \bar{\nabla}^i \bar{\nabla}_i$  is the Laplacian operator associated with the flat 3-metric  $f_{ij}$ .

Apart from the gravitational field equations, we have to solve the fluid equations simultaneously. The equations governing the quasiequilibrium state are the Euler equation and the equation of continuity. The first integral of the Euler equation is written as

$$H + \nu - \ln \Gamma_0 + \ln \Gamma = \text{constant}, \quad (11)$$

where  $H := \ln h$  is the logarithm of the fluid specific enthalpy:

$$h := \frac{e + p}{m_B n}, \quad (12)$$

$m_B$  being the mean baryon mass. Here  $\Gamma_0$  is the Lorentz factor between the co-orbiting observer whose 4-velocity is  $v_\mu$  and the Eulerian observer:

$$\Gamma_0 := -n^\mu v_\mu, \quad (13)$$

and  $\Gamma$  is that between the fluid and the co-orbiting observer:

$$\Gamma := -v^\mu u_\mu. \quad (14)$$

The equation of continuity is written as

$$\zeta H \underline{\Delta} \Psi + \bar{\nabla}^i H \bar{\nabla}_i \Psi = A^2 h \Gamma_n U_0^i \bar{\nabla}_i H + \zeta H [\bar{\nabla}^i \Psi \bar{\nabla}_i (H - \beta) + A^2 h U_0^i \bar{\nabla}_i \Gamma_n], \quad (15)$$

where  $\Psi$  is the velocity potential and  $\zeta$  the thermodynamical coefficient:

$$\zeta := \frac{d \ln H}{d \ln n}. \quad (16)$$

$\Gamma_n$  denotes the Lorentz factor between the fluid and the Eulerian observer:

$$\Gamma_n := -n^\mu u_\mu, \quad (17)$$

and  $U_0^i$  is the orbital 3-velocity with respect to the Eulerian observer:

$$U_0^i = -\frac{B^i}{N}. \quad (18)$$

The three Lorentz factors are expressed in the IWM approximation as

$$\Gamma_0 = (1 - A^2 f_{ij} U_0^i U_0^j)^{-1/2}, \quad (19)$$

$$\Gamma_n = (1 - A^2 f_{ij} U^i U^j)^{-1/2}, \quad (20)$$

$$\Gamma = \Gamma_n \Gamma_0 (1 - A^2 f_{ij} U^i U_0^j), \quad (21)$$

where  $U^i$  is the fluid 3-velocity with respect to the Eulerian observer, which is written as  $U^i = U_0^i$  for synchronized binary systems and as

$$U^i = \frac{1}{A^2 \Gamma_n h} \bar{\nabla}^i \Psi \quad (22)$$

for irrotational ones.

### C. Numerical method

Before going further, it might be instructive to shortly recall the numerical method and the special technique to treat the case of non-integer polytropic index  $n = 1/(\gamma - 1)$  [24, 61].

Through the series of works, we have developed a numerical code which is based on a multidomain spectral method with surface-fitted coordinates [62, 63]. The numerical code is constructed upon the C++ library LORENE [64].

One of the merits of considering multiple domains is that to allow for boundary conditions at infinity, by compactifying the outermost domain. Another merit is that we can separate the region including baryon from other ones. This property results in accurate computations, because if there is a large gap in some physical quantity, for example, the baryon density, which is treated in one domain, its spectral expansion produces unphysical oscillations, i.e., Gibbs phenomena. However, even though the region including baryon density is divided from the others, the Gibbs phenomenon will happen if the baryon density profile has a stiff equation of state. In the case of polytrope, the first derivative of density at the stellar surface diverges for adiabatic indices larger than 2. (Even for  $\gamma < 2$ , if the polytropic index ( $n$ ) is not an integer, higher derivatives of density at the stellar surface diverge.) In order to overcome this type of Gibbs phenomenon, we have introduced a regularization technique in Ref. [61] and Paper II.

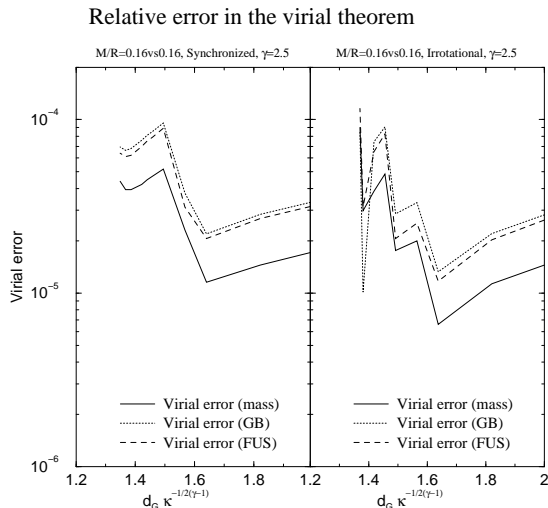


FIG. 1: Relative error in the virial theorem of stationary figures in general relativity as a function of the orbital separation. Solid, dotted, and dashed lines denote the relative errors in mass, of Gourgoulhon and Bonazzola, and of Friedman, Uryu, and Shibata, respectively. Left (right) panel is for synchronized (irrotational) binary systems. Both of them are calculated for the identical-mass binary system with the adiabatic index  $\gamma = 2.5$  and the compactness  $M/R = 0.16$  vs  $0.16$ .

### III. CODE TESTS

Numerous tests have already been shown in previous articles [24, 25, 34, 35]. In the present article, then, we presents tests only regarding (i) the global numerical error measured by the virial theorem, (ii) the numerical error in the first law of binary neutron star thermodynamics [44], (iii) the comparison with previous numerical solutions, and (iv) the convergence to post-Newtonian results at large separation. This last type of test will be presented in Sec. IV C (see Figs. 25 – 26); here we focus on the virial theorem and the first law of binary neutron star thermodynamics. The former has proved to be useful to check the global error in numerical solutions for stationary fluid systems. A general relativistic version of the virial theorem has been obtained by Gourgoulhon and Bonazzola [65] for stationary spacetimes. It has been recently extended to binary star spacetimes within the IWM approximation by Friedman, Uryu and Shibata [44]<sup>4</sup>. The virial relation is equivalent to require

$$M_{\text{ADM}} = M_{\text{Komar}}, \quad (23)$$

<sup>4</sup> The spacetime generated by a binary system is not stationary, due to gravitational radiation. However, within the IWM approximation, the gravitational radiation is neglected in the global spacetime dynamics, so that one is able to recover the virial theorem.

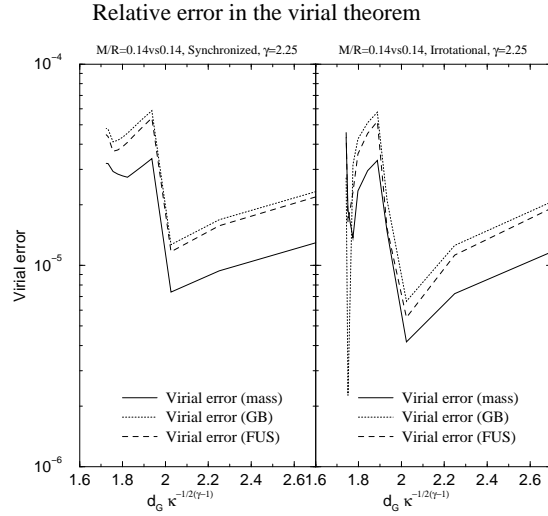


FIG. 2: Same as Fig. 1 but for  $\gamma = 2.25$  and  $M/R = 0.14$  vs 0.14.

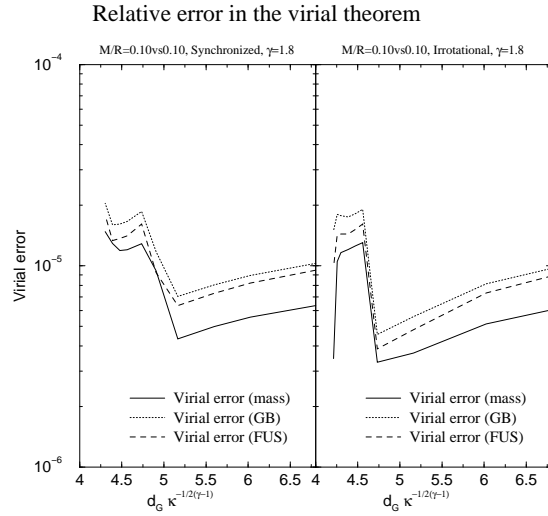


FIG. 3: Same as Fig. 1 but for  $\gamma = 1.8$  and  $M/R = 0.10$  vs 0.10.

where  $M_{\text{ADM}}$  is the ADM mass:

$$M_{\text{ADM}} = -\frac{1}{2\pi} \oint_{\infty} \bar{\nabla}^i A^{1/2} dS_i, \quad (24)$$

and  $M_{\text{Komar}}$  is a Komar-type mass, defined by

$$M_{\text{Komar}} = \frac{1}{4\pi} \oint_{\infty} \bar{\nabla}^i N dS_i. \quad (25)$$

The virial theorem obtained by Friedman, Uryu and Shibata [44] (see also Eq. (5.7) of Ref. [46]) writes

$$\begin{aligned} VE(FUS) &= \int \left[ 2NA^3S + \frac{3}{8\pi} NA^3 K_i^j K_j^i + \frac{1}{4\pi} NA(\bar{\nabla}_i \beta \bar{\nabla}^i \beta - \bar{\nabla}_i \nu \bar{\nabla}^i \nu) \right] d^3x \\ &= 0. \end{aligned} \quad (26)$$

By a straightforward manipulation, this integral can be recast in the form of the virial theorem as obtained by Gourgoulhon and Bonazzola [65]:

$$\begin{aligned} VE(GB) &= \int \left[ 2A^3 S + \frac{3}{8\pi} A^3 K_i^j K_j^i + \frac{1}{4\pi} A (\nabla_i \beta \nabla^i \beta - \nabla_i \nu \nabla^i \nu - 2 \nabla_i \beta \nabla^i \nu) \right] d^3 x \\ &= 0. \end{aligned} \quad (27)$$

Let us stress that the above identity has been derived by Gourgoulhon and Bonazzola [65] only for stationary spacetimes and that its validity for IWM spacetimes with helical Killing vector has been obtained by Friedman, Uryu and Shibata [44].

As error indicators of our numerical solutions, we have evaluated the quantities

$$\left| \frac{M_{\text{ADM}} - M_{\text{Komar}}}{M_{\text{ADM}}} \right|, \quad (28)$$

$$\left| \frac{VE(FUS)}{M_{\text{ADM}}} \right|, \quad (29)$$

$$\left| \frac{VE(GB)}{M_{\text{ADM}}} \right|. \quad (30)$$

The results are presented in Figs. 1 – 3 as a function of the orbital separation. In each figure, the left panel is for the synchronized case, and the right one for the irrotational case. The vertical axis denotes the relative virial errors defined by Eqs. (28)-(30). One can notice in these panels a sudden change in the slope of the lines around the middle of the sequences. This is due to the fact that we use five computational domains for each star and the space around it in the case of large separation and four domains for small separation, inducing a change in the accuracy of the computation. However, since such discrete changes are only factor two or three better even if we use five computational domains for close separation, we decided to use four domains in order to save computational time. The order of magnitude of the virial error is  $\sim 10^{-5}$  through the sequence. This is sufficient to discuss the physics of binary systems accurately.

The first law of binary neutron star thermodynamics for the IWM approximation has also been derived by Friedman, Uryu and Shibata [44]. It is written as

$$\delta M_{\text{ADM}} = \Omega \delta J, \quad (31)$$

where  $\delta M_{\text{ADM}}$  and  $\delta J$  are respectively the changes in ADM mass and angular momentum along a constant baryon number sequence, and  $\Omega$  denotes the orbital angular velocity. The relative error  $|(\delta M_{\text{ADM}} - \Omega \delta J) / \delta M_{\text{ADM}}|$  is calculated for some selected points in the sequences by using a second order polynomial fitting. It is found that the relative error is better than a few of  $10^{-3}$  for large separations and  $1 \times 10^{-2}$  for medium separations. However, it becomes a few % or worse for close separations and around the turning point of the ADM mass.

Next, we have compared our results with the irrotational sequences computed by Uryu, Shibata and Eriguchi [37]. Since only data at the sequence end points are listed in Ref. [37], we have compared for end point configurations only. It is found that the ADM mass agree with each other at the order of  $10^{-3}$ , and the orbital angular velocity and the total angular momentum agree at a few %.

#### IV. NUMERICAL RESULTS

In this section, we show the results of numerical computations. The number of collocation points of spectral method which we choose in the present paper is  $N_r \times N_\theta \times N_\varphi = 25 \times 17 \times 16$  or  $33 \times 25 \times 24$ , where  $N_r$ ,  $N_\theta$ , and  $N_\varphi$  denote the number of collocation points to the radial, the polar, and the azimuthal directions. The number of spectral domains which we use for each star and the space around it is five (resp. four) in the case of a large (resp. small) separation.

As in Paper III, we parametrize the difference in baryon mass between the two stars in a binary system by the values of compactness of stars like  $[(M/R)_{\infty, \text{star 1}} \text{ vs } (M/R)_{\infty, \text{star 2}}]$ , where  $(M/R)_\infty$  denotes the compactness of an isolated spherical star with the same baryon number. Hereafter, we abbreviate  $(M/R)_{\infty, \text{star 1}} \text{ vs } (M/R)_{\infty, \text{star 2}}$  as  $M/R$  for simplicity. According to recent nuclear physics equations of state, the compactness of a  $M = 1.4 M_\odot$  neutron star is in the range  $0.12 \leq M/R \leq 0.20$ , depending on the equation of state [53]. We therefore explore this range of compactness for our polytropic equations of state. We display the compactness parameters used for each adiabatic index  $\gamma$  in Fig. 4. For each couple of values  $(\gamma, M/R)$ , one can see in Fig. 4 how far the considered model is from the maximum mass configuration.

Since we have already shown numerous results for  $\gamma = 2$  in Paper III, we concentrate on the results for  $\gamma = 2.5$ , 2.25, and 1.8. For the adiabatic index  $\gamma = 3$ , we present one of results in Sec. V, because the value  $\gamma = 3$  is too large for the equation of state of neutron stars.

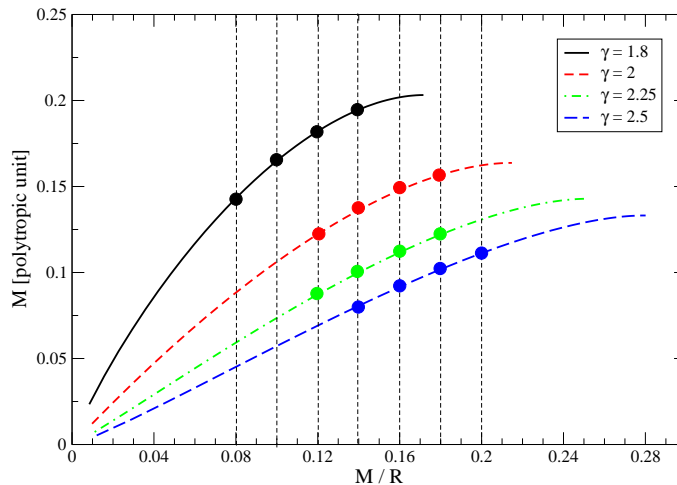


FIG. 4: Single non-rotating neutron star models in the compactness - gravitational mass plane. The right end of each curve is the maximum mass model. The gravitational mass  $M$  is rescaled by the polytropic constant  $\kappa$ :  $\bar{M} = \kappa^{-1/(2(\gamma-1))} M$ . The dots correspond to values of compactness for the binary systems computations performed in the present work.

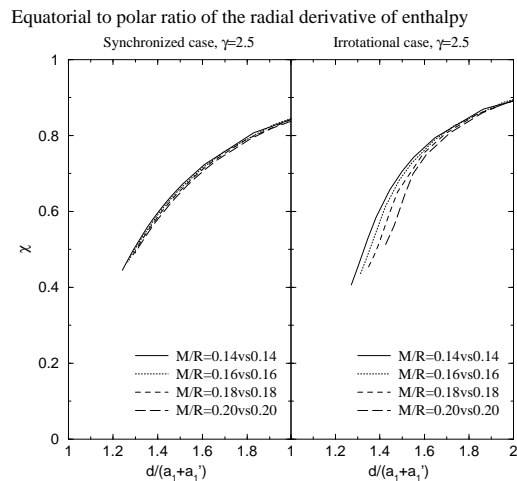


FIG. 5: Equatorial to polar ratio of the radial derivative of the enthalpy as a function of the orbital separation. Left (right) panel is for synchronized (irrotational) binary systems with the adiabatic index  $\gamma = 2.5$ . Solid, dotted, dashed, and long-dashed lines denote the cases of the compactness  $M/R = 0.14$  vs  $0.14$ ,  $0.16$  vs  $0.16$ ,  $0.18$  vs  $0.18$ , and  $0.20$  vs  $0.20$ , respectively.

### A. End points of sequences

First of all, equatorial to polar ratios of the radial derivative of the enthalpy

$$\chi := \frac{(\partial H / \partial r)_{\text{eq,comp}}}{(\partial H / \partial r)_{\text{pole}}} \quad (32)$$

are shown in Figs. 5 – 7 for identical-mass binary systems and in Figs. 8 – 10 for different-mass systems compared with identical-mass ones. This quantity is a good dimensionless indicator to detect the appearance of cusp at the stellar surface, which corresponds to the mass-shedding limit. The horizontal axis presents the orbital coordinate separation between the two coordinate centers (maximum of density) ( $d$ ) normalized by the summation of the coordinate radii of stars in the direction of their companions ( $a_1$  and  $a'_1$ ), where the prime denotes the quantity concerned with the more massive star. The dimensionless quantity  $d/(a_1 + a'_1)$  is an indicator of the contact of two stars. If it takes unity, the two stars contact with each other. Note here that  $d$ ,  $a_1$ , and  $a'_1$  are all coordinate lengths.

From Figs. 5 – 7, one can see that the lines seem to focus on the point  $d/(a_1 + a'_1) = 1$  and  $\chi = 0$  in the case of synchronized binary systems. This implies that the synchronized binary systems of identical-mass stars in

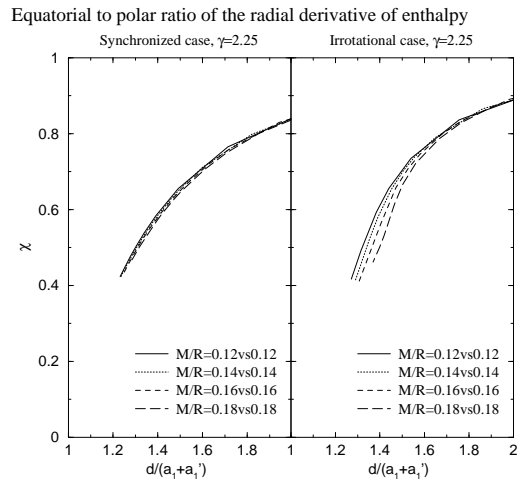


FIG. 6: Same as Fig. 5 but for  $\gamma = 2.25$ . Solid, dotted, dashed, and long-dashed lines denote the cases of the compactness  $M/R = 0.12$  vs  $0.12$ ,  $0.14$  vs  $0.14$ ,  $0.16$  vs  $0.16$ , and  $0.18$  vs  $0.18$ , respectively.

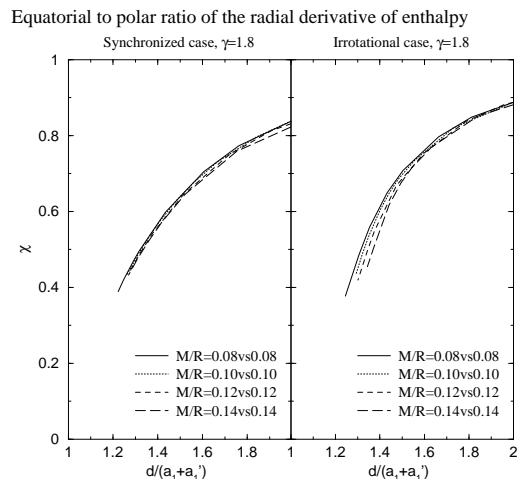


FIG. 7: Same as Fig. 5 but for  $\gamma = 1.8$ . Solid, dotted, dashed, and long-dashed lines denote the cases of the compactness  $M/R = 0.08$  vs  $0.08$ ,  $0.10$  vs  $0.10$ ,  $0.12$  vs  $0.12$ , and  $0.14$  vs  $0.14$ , respectively.

quasiequilibrium end their sequences at the contact point of two stars. It is worth to point out that the lines for all cases of compactness in the figures take almost the same tracks, but very slightly deviate from each other. The lines of larger compactness are located below those of smaller compactness in the figures. On the other hand, in the case of irrotational binary systems, the lines seem to reach  $\chi = 0$  at  $d/(a_1 + a'_1) > 1$ . This means that the end point of quasiequilibrium sequences of irrotational binary systems is a cusp point. This tendency is enhanced for the case of larger compactness. Note here that in Figs. 5 and 6, the lines with larger compactness in the case of irrotational binary systems turn slightly to the vertical axis around  $\chi \sim 0.5$ . This comes from the numerical error. The real quasiequilibrium sequences should exist up to  $\chi = 0$ . However, the spectral method we employ cannot handle cusplike figures because of the Gibbs phenomena. Accordingly, in the numerical computations, the difference of the enthalpy between two successive computational steps  $\delta H$  hardly goes below  $10^{-5}$  for synchronized binary systems when the orbital separation is such that  $\chi \sim 0.4$ . For irrotational ones, although it is still possible to reach  $\delta H \sim 10^{-6}$  when the orbital separation is such that  $\chi \sim 0.4 - 0.5$ , unphysical oscillations of the stellar surface appear. This produces the unphysical turn in the lines of irrotational binary systems. These tendencies are enhanced for more stiff equation of state (larger adiabatic index  $\gamma$ ) and more compact stars (larger compactness  $M/R$ ). Therefore, we stop the computations around  $\chi \sim 0.4 - 0.5$ .

We compare the equatorial to polar ratio of the radial derivative of the enthalpy in the different-mass case with

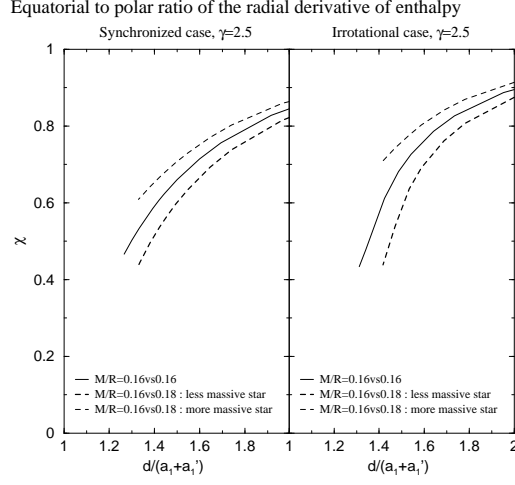


FIG. 8: Same as Fig. 5 but for different-mass binary systems compared with an identical-mass binary system. The solid line denotes the case of identical-mass binary system with the compactness  $M/R = 0.16$  vs  $0.16$ . Thin and thick dashed lines are, respectively, for the more massive and less massive stars of different-mass binary system with  $M/R = 0.16$  vs  $0.18$ .

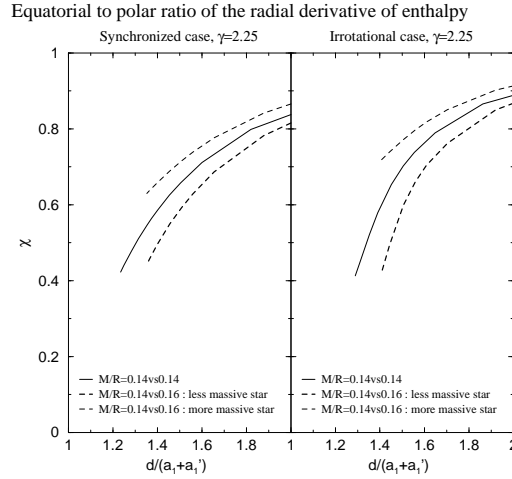


FIG. 9: Same as Fig. 8 but for  $\gamma = 2.25$ . The solid line denotes the case of identical-mass binary system with the compactness  $M/R = 0.14$  vs  $0.14$ . Thin and thick dashed lines are, respectively, for the more massive and less massive stars of different-mass binary system with  $M/R = 0.14$  vs  $0.16$ .

that in the identical-mass one in Figs. 8 – 10. One can see from these figures that the sequences seem to terminate by a cusp point of the less massive star for both synchronized and irrotational binary systems when we extrapolate the lines, while the more massive star keeps its shape near a spherical one. It is worth to note here that as soon as the two masses differ, even slightly, the sequence of a synchronized binary system terminates by a cusp point, because the line for the less massive star is always located below that for the identical-mass stars which will reach  $\chi = 0$  at  $d/(a_1 + a'_1) = 1$ . This implies that the line for the less massive star seems to always reach  $\chi = 0$  at  $d/(a_1 + a'_1) > 1$ .

In Fig. 11, the equatorial to polar ratio of the radial derivative of the enthalpy is shown by fixing the compactness parameter as  $M/R = 0.14$  vs  $0.14$  and varying adiabatic index. It is clearly found that the lines in the case of smaller adiabatic index are located below those in the larger adiabatic case. This means that the case of smaller adiabatic index is closer to the mass-shedding point compared with that of higher one when we fix the relative orbital separation. The reason is that the stars of smaller adiabatic index have centrally concentrated structures with extended low density halo. Such low density outer layers lead to smaller  $\chi$ .

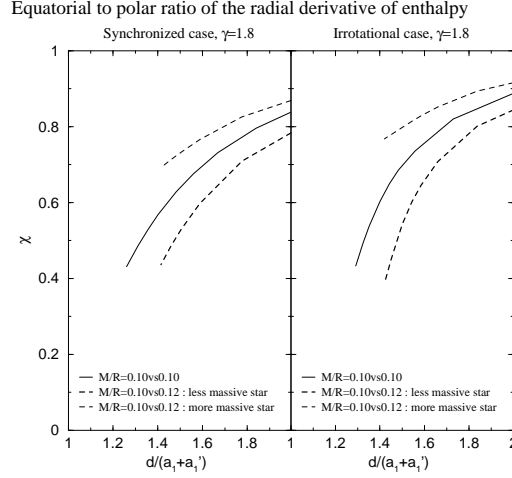


FIG. 10: Same as Fig. 8 but for  $\gamma = 1.8$ . The solid line denotes the case of identical-mass binary system with the compactness  $M/R = 0.10$  vs  $0.10$ . Thin and thick dashed lines are, respectively, for the more massive and less massive stars of different-mass binary system with  $M/R = 0.10$  vs  $0.12$ .

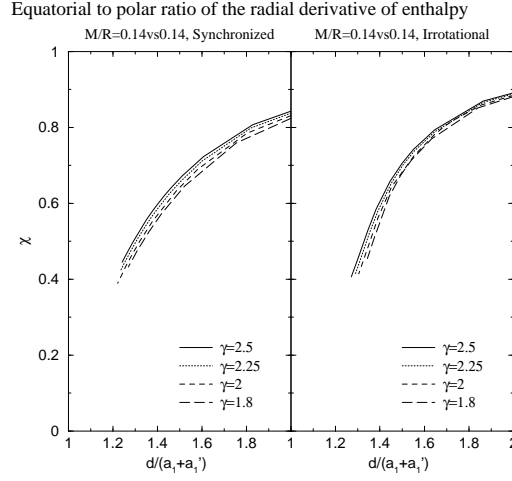


FIG. 11: Equatorial to polar ratio of the radial derivative of the enthalpy as a function of the orbital separation. Left (right) panel is for synchronized (irrotational) binary systems with the compactness  $M/R = 0.14$  vs  $0.14$ . Solid, dotted, dashed, and long-dashed lines denote the cases of adiabatic indices  $\gamma = 2.5, 2.25, 2,$  and  $1.8$ , respectively.

### B. Relative change in central energy density

Secondarily, we represent the relative change in central energy density in Figs. 12 – 14. In these figures,  $e_c$  and  $e_{c,\infty}$  denote the central energy density of a star and that of an isolated spherical star with the same baryon mass, respectively. One can see from these figures that all sequences decrease their central energy densities as the orbital separation decreases. It is also found that the amount of decrease of the central energy density is larger for larger compactness when we fix the adiabatic index and the rotation state. Note here that the order of amount of the decrease is completely different between the synchronized case and the irrotational one. The central energy density of synchronized binary systems decreases about 10 %, while that of irrotational ones does only a few %.

While the relative change in central energy density is shown as a function of the orbital separation in Figs. 12 – 14, it is presented as a function of the cusp indicator  $\chi$  in Figs. 15 – 17, because it is convenient to see the change at the end point of the sequence and how to split the lines of various compactness. It is found from these figures that the central energy density in the case of larger compactness decreases larger than that of smaller compactness. Furthermore, we can see that the decreasing track of central energy density is determined by the compactness of the

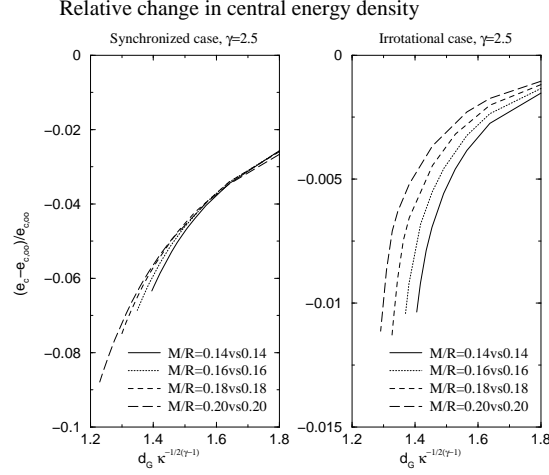


FIG. 12: Relative change in central energy density as a function of the orbital separation between the centers of mass of each star. Left (right) panel is for synchronized (irrotational) binary systems with the adiabatic index  $\gamma = 2.5$ . Solid, dotted, dashed, and long-dashed lines denote the cases of identical-mass binary systems with the compactness  $M/R = 0.14$  vs  $0.14$ ,  $0.16$  vs  $0.16$ ,  $0.18$  vs  $0.18$ , and  $0.20$  vs  $0.20$ , respectively.

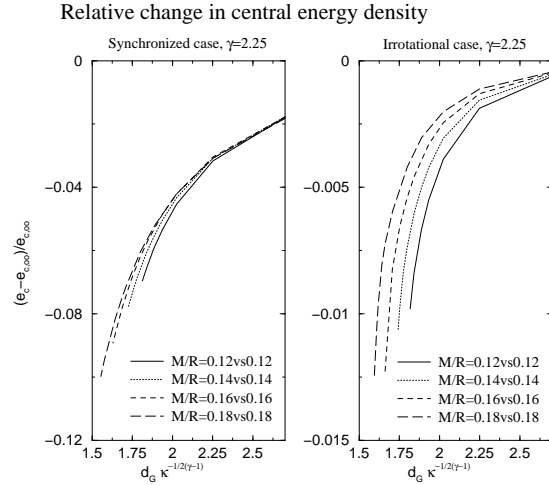


FIG. 13: Same as Fig. 12 but for  $\gamma = 2.25$ . Solid, dotted, dashed, and long-dashed lines denote the cases of identical-mass binary systems with the compactness  $M/R = 0.12$  vs  $0.12$ ,  $0.14$  vs  $0.14$ ,  $0.16$  vs  $0.16$ , and  $0.18$  vs  $0.18$ , respectively.

star itself not by that of the companion star, even though the value itself is affected by the companion star. This effect is clearly found for the synchronized binary systems. Since the amount of decrease is very small for irrotational binary systems and the lines include numerical errors, it is not clear that the decrease depends only on the compactness of the star not on that of the companion star. However, it could be found the tendency in particular in the case of soft equation of state like  $\gamma = 1.8$  (see Fig. 17). Note here that the turn of lines at  $\chi \sim 0.5$  for larger compactness in the irrotational case in Figs. 15 and 16 comes from numerical error which is explained in the previous subsection IV A.

Although the sequences stop at around  $\chi \simeq 0.4$ , it is possible to predict how much the central energy density decreases at the end of sequences by extrapolating the lines in Figs. 15 – 17. For example, the central energy density of synchronized binary systems with  $\gamma = 2.25$  may decrease about 10 % – 15 % in the range of  $M/R = 0.12$  vs  $0.12$  –  $0.18$  vs  $0.18$ .

Figure 18 is shown in order to investigate the behavior of the relative change in central energy density varying adiabatic index fixing the compactness. It is found that the rate of decrease is lower for larger adiabatic index. This is because the larger adiabatic index implies closer to the “incompressible” state in which the central energy density does not change.

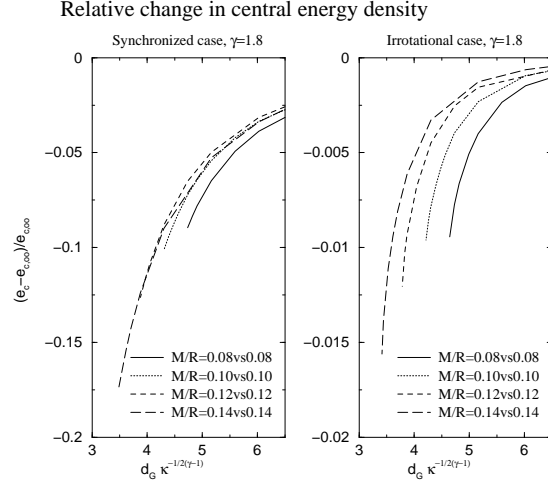


FIG. 14: Same as Fig. 12 but for  $\gamma = 1.8$ . Solid, dotted, dashed, and long-dashed lines denote the cases of identical-mass binary systems with the compactness  $M/R = 0.08$  vs  $0.08$ ,  $0.10$  vs  $0.10$ ,  $0.12$  vs  $0.12$ , and  $0.14$  vs  $0.14$ , respectively.

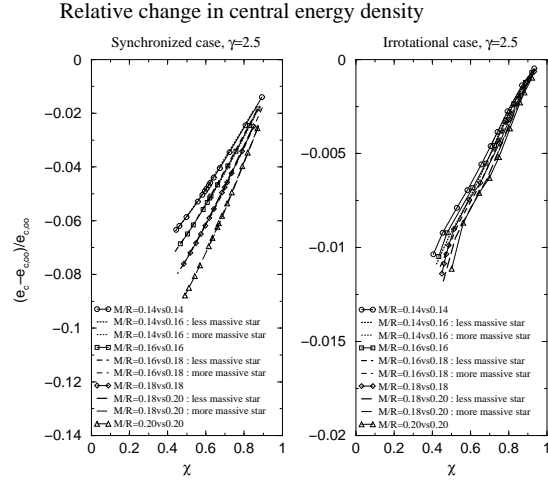


FIG. 15: Relative change in central energy density as a function of the cusp indicator  $\chi$ . Left (right) panel is for synchronized (irrotational) binary systems with the adiabatic index  $\gamma = 2.5$ . Solid lines with open circle, square, diamond, and triangle denote the cases of identical-mass binary systems of compactness  $M/R = 0.14$  vs  $0.14$ ,  $0.16$  vs  $0.16$ ,  $0.18$  vs  $0.18$ , and  $0.20$  vs  $0.20$ , respectively. Thick and thin dotted lines are for the less and more massive stars of the different-mass binary system of  $M/R = 0.14$  vs  $0.16$ , thick and thin dashed lines for those of  $M/R = 0.16$  vs  $0.18$ , and thick and thin long-dashed lines for those of  $M/R = 0.18$  vs  $0.20$ , respectively.

### C. ADM mass and total angular momentum

Thirdly, the ADM mass and the total angular momentum as a function of the orbital angular velocity are presented in Figs. 19 – 21 and Figs. 22 – 24. These figures show that the turning points appear once for the synchronized case with  $\gamma = 2.5$  and  $2.25$ . On the other hand, we cannot find it in the synchronized case with  $\gamma = 1.8$  and in the irrotational case. Note that the position of the apparition of the turning point in the ADM mass and the total angular momentum is coincide with each other, as expected [44]. The turning points are also found in the different-mass case for synchronized binary systems with  $\gamma = 2.5$  and  $2.25$ . However, the position is closer to the end point of the sequence than that in the identical-mass case. Since we stop computing before the end point of quasiequilibrium sequences as mentioned above, there is a possibility that the turning point may exist in the range of  $0 < \chi < 0.4$ , even if we do not find it in the synchronized case with  $\gamma = 1.8$  and in the irrotational case. The total understanding of the apparition of the turning point for various adiabatic indices and compactness will be discussed later in Sec. V.

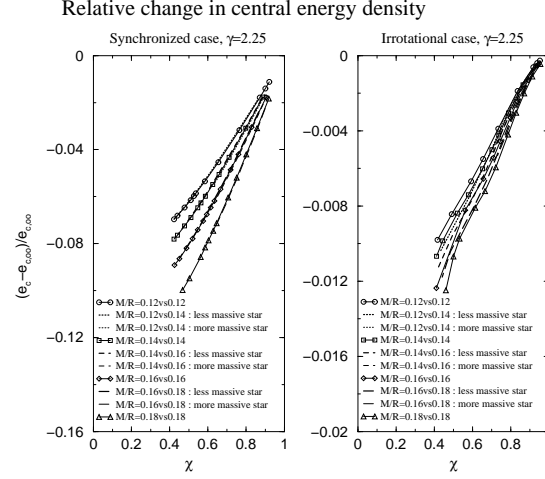


FIG. 16: Same as Fig. 15 but for  $\gamma = 2.25$ . Solid lines with open circle, square, diamond, and triangle denote the cases of identical-mass binary systems of compactness  $M/R = 0.12$  vs  $0.12$ ,  $0.14$  vs  $0.14$ ,  $0.16$  vs  $0.16$ , and  $0.18$  vs  $0.18$ , respectively. Thick and thin dotted lines are for the less and more massive stars of the different-mass binary system of  $M/R = 0.12$  vs  $0.14$ , thick and thin dashed lines for those of  $M/R = 0.14$  vs  $0.16$ , and Thick and thin long-dashed lines for those of  $M/R = 0.16$  vs  $0.18$ , respectively.

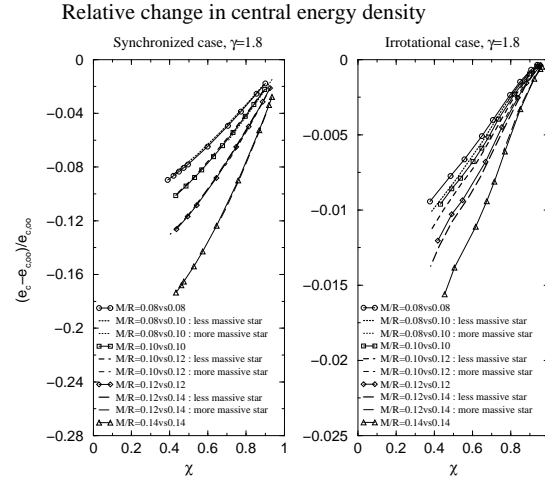


FIG. 17: Same as Fig. 15 but for  $\gamma = 1.8$ . Solid lines with open circle, square, diamond, and triangle denote the cases of identical-mass binary systems of compactness  $M/R = 0.08$  vs  $0.08$ ,  $0.10$  vs  $0.10$ ,  $0.12$  vs  $0.12$ , and  $0.14$  vs  $0.14$ , respectively. Thick and thin dotted lines are for the less and more massive stars of the different-mass binary system of  $M/R = 0.08$  vs  $0.10$ , Thick and thin dashed lines for those of  $M/R = 0.10$  vs  $0.12$ , and Thick and thin long-dashed lines for those of  $M/R = 0.12$  vs  $0.14$ , respectively.

In Figs. 25 – 26, we present the ADM mass as a function of the orbital angular velocity, as in Figs. 19 – 21, but with a scaling defined by twice the gravitational mass of the single static neutron star of the same baryon number as that of the sequence,  $M_0$ , whereas in Figs. 19 – 21, the scaling was set by the polytropic constant  $\kappa$ . Note that  $M_0$  can also be viewed as the ADM mass at infinite separation. This enables us to compare with third order post-Newtonian results for point-mass particles obtained in the Effective One Body (EOB) approach by Damour et al. [66, 67] or in the standard non-resummed post-Newtonian framework by Blanchet [68]. This also enables us to compare with corotating binary black holes, according to the numerical results by Grandclément et al. [69]. We note from these figures that the irrotational binary neutron star sequences are very close to the 3PN irrotational ones (dashed and dotted fine lines). Moreover, all curves converges at large separation (small value of  $\Omega M_0$ ), which can be considered as a check of our numerical computations. Another interesting feature shown in Fig. 25 is the good agreement between the irrotational binary neutron star sequence with high compactness ( $M/R = 0.20$ ) and the binary black hole sequence. The latter is

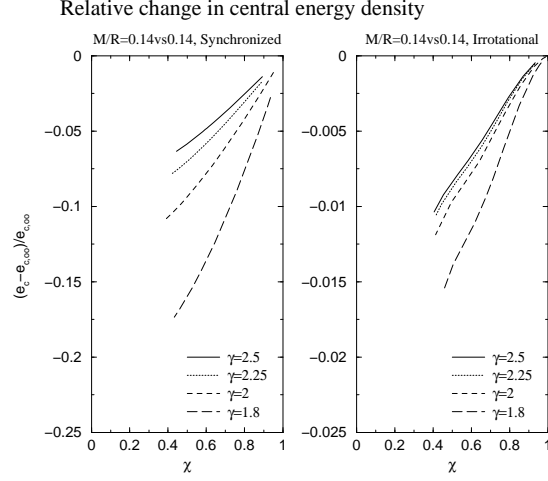


FIG. 18: Relative change in central energy density as a function of the cusp indicator  $\chi$ . Left (right) panel is for synchronized (irrotational) binary systems with the compactness  $M/R = 0.14$  vs  $0.14$ . Solid, dotted, dashed, and long-dashed lines denote the cases of  $\gamma = 2.5, 2.25, 2,$  and  $1.8$ , respectively.

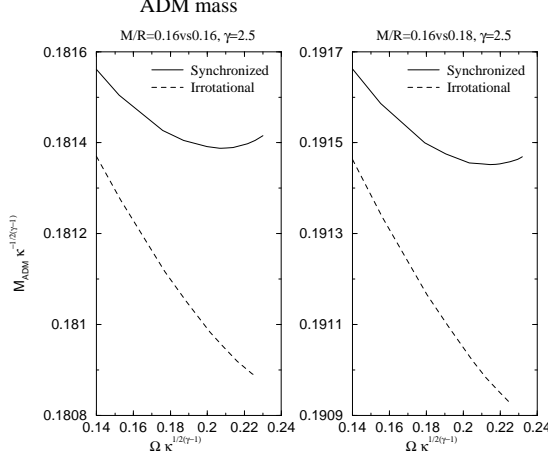


FIG. 19: ADM mass of the binary system as a function of the orbital angular velocity. Left (right) panel is for identical-mass (different-mass) binary systems of compactness  $M/R = 0.16$  vs  $0.16$  ( $M/R = 0.16$  vs  $0.18$ ) with the adiabatic index  $\gamma = 2.5$ . In each panel, the solid line denotes the synchronized case, and the dashed the irrotational one.

made of corotating black holes, but for  $\Omega M_0 \leq 0.06$ , the spin effects are not very important, so that it is meaningful to compare the corotating black hole sequence up to  $\Omega M_0 \leq 0.06$  with the irrotational neutron star sequence. Finally, we notice from Fig. 26 that at a given compactness and separation, the configuration with smaller adiabatic index is more bound. Conversely, at a given adiabatic index and separation, the configuration with higher compactness is more bound.

#### D. Axial ratios

Fourthly, the axial ratios are presented in Figs. 27 – 29. In these figures, we depict the lines as a function of the quantity  $\chi$ . This expression has an advantage in which we can speculate the values of the axial ratios at the end point of the sequence, because the figures have linear-like lines. Since the value  $\chi = 0$  corresponds to the end point of the sequence, we can imagine how much the stars deform at the end of the sequence if we extrapolate the lines to  $\chi = 0$ . It is also possible to perceive that the configuration of stars with larger compactness is closer to the spherical figure than smaller compactness when we compare it at the same  $\chi$ . Extrapolating the lines in the figures, the axial

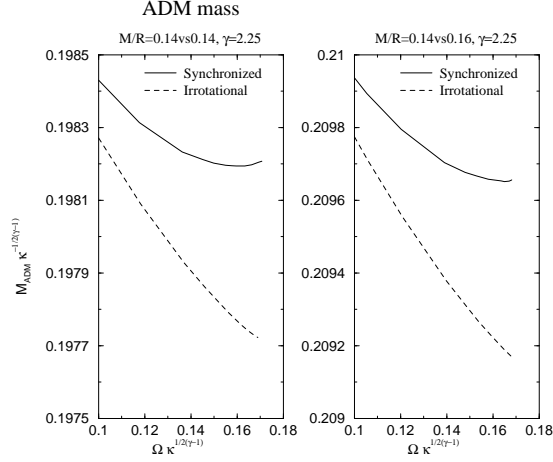


FIG. 20: Same as Fig. 19 but for  $\gamma = 2.25$ . Left (right) panel is for identical-mass (different-mass) binary systems of compactness  $M/R = 0.14$  vs  $0.14$  ( $M/R = 0.14$  vs  $0.16$ ).

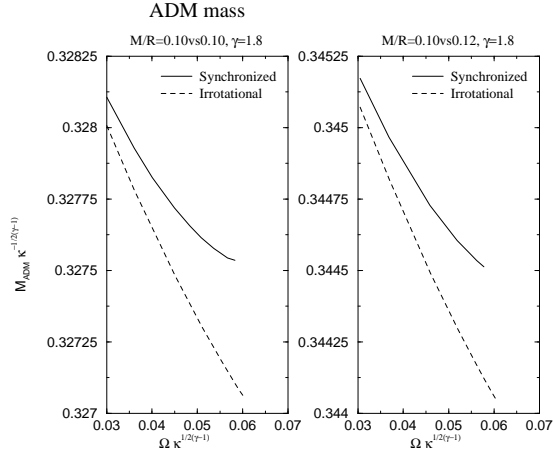


FIG. 21: Same as Fig. 19 but for  $\gamma = 1.8$ . Left (right) panel is for identical-mass (different-mass) binary systems of compactness  $M/R = 0.10$  vs  $0.10$  ( $M/R = 0.10$  vs  $0.12$ ).

ratios at the end point of sequences are predicted as  $a_2/a_1 \sim 0.7$  and  $a_3/a_1 \sim 0.6$  for synchronized binary systems with  $\gamma = 2.5$ , and  $a_2/a_1 \sim 0.67 - 0.72$  and  $a_3/a_1 \sim 0.7 - 0.75$  for irrotational ones with  $\gamma = 2.5$ . Note here that the turn of lines at  $\chi \sim 0.5$  for larger compactness in the irrotational case in Figs. 27 and 28 comes from numerical error which is explained in the previous subsection IV A.

We also present the change of the axial ratios along the sequence in Fig. 30 by fixing the compactness and varying adiabatic index. It is clearly seen from this figure that that the deformation of the star is larger for larger adiabatic index.

### E. Contours of baryon density, shift vectors, and velocity fields

Isocontours of the baryon density of various binary systems are shown in Figs. 31 – 36. There are two panels in each figures. The left panel shows the result for identical-mass binary system, while the right one is that for different-mass binary system. In the right panel in each figure, the left-hand side star is the less massive star. It is clearly seen that the less massive star is tidally deformed and elongated while the more massive star relatively does not deviate from the spherical shape so much.

The shift vector  $N^i$  of nonrotating coordinates is shown in Fig. 37 for both synchronized and irrotational binary

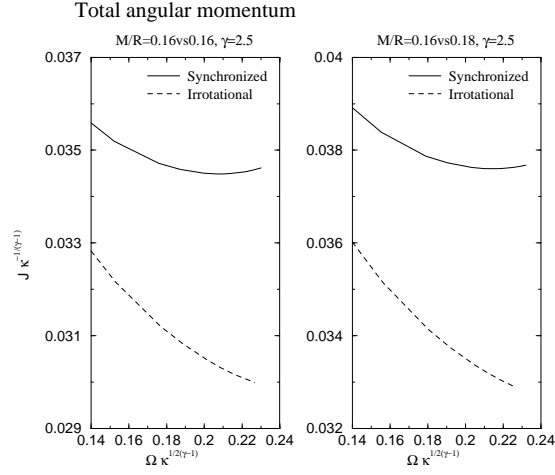


FIG. 22: Total angular momentum of the binary system as a function of the orbital angular velocity. Left (right) panel is for identical-mass (different-mass) binary systems of compactness  $M/R = 0.16$  vs  $0.16$  ( $M/R = 0.16$  vs  $0.18$ ) with the adiabatic index  $\gamma = 2.5$ . In each panel, the solid line denotes the synchronized case, and the dashed the irrotational one.

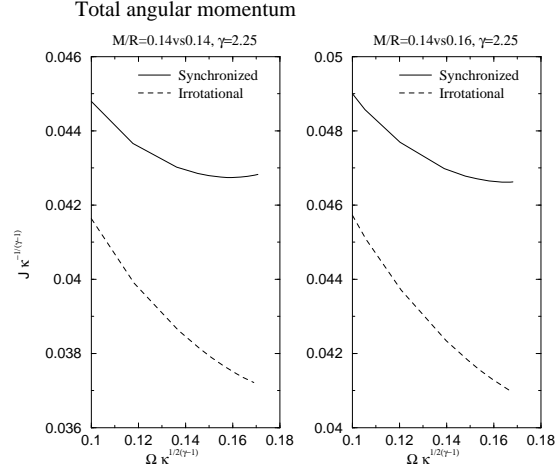


FIG. 23: Same as 22 but for  $\gamma = 2.25$ . Left (right) panel is for identical-mass (different-mass) binary systems of compactness  $M/R = 0.14$  vs  $0.14$  ( $M/R = 0.14$  vs  $0.16$ ).

systems with  $\gamma = 2.25$  in the case of compactness  $M/R = 0.14$  vs  $0.16$ . The plot is a cross section of the orbital plane.

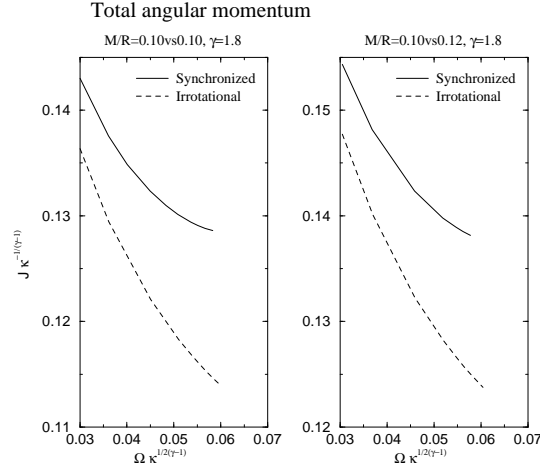


FIG. 24: Same as 22 but for  $\gamma = 1.8$ . Left (right) panel is for identical-mass (different-mass) binary systems of compactness  $M/R = 0.10$  vs  $0.10$  ( $M/R = 0.10$  vs  $0.12$ ).

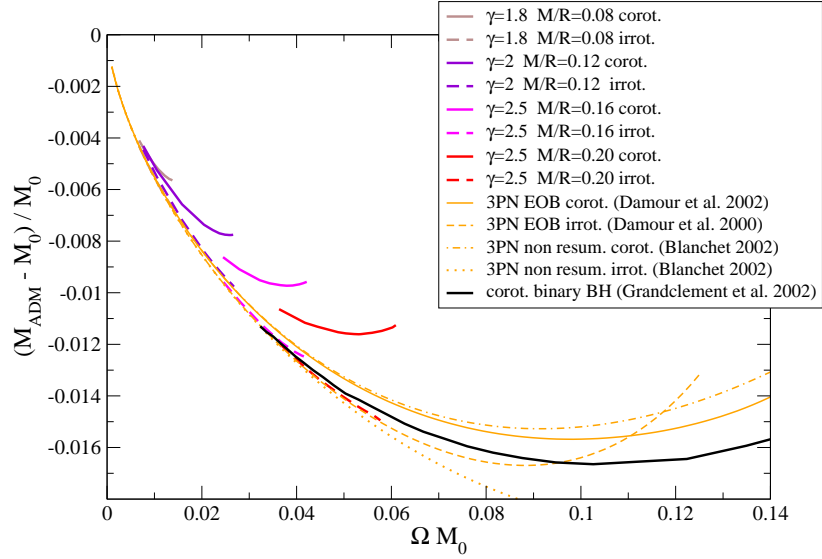


FIG. 25: Relative binding energy along evolutionary sequences of equal-mass binary neutron stars, compared with (i) analytical results at the 3rd post-Newtonian order for point-masses by Damour et al. 2000 [66], Damour et al. 2002 [67] and Blanchet 2002 [68], and with (ii) numerical results for corotating binary black holes by Grandclément et al. 2002 [69].  $\Omega$  is the orbital angular velocity and  $M_0$  is twice the gravitational mass of a single static neutron star (resp. black hole) of the same baryon number (resp. same horizon area) as that of the considered sequence.

In Fig. 38, the velocity field in the Eulerian frame  $U^i$  is presented for both synchronized and irrotational binary systems with  $\gamma = 2.25$  in the case of compactness  $M/R = 0.14$  vs  $0.16$ .

The internal velocity field in the co-orbiting frame is shown in Fig. 39 for the irrotational binary system with  $\gamma = 2.25$  in the case of compactness  $M/R = 0.14$  vs  $0.16$ .

## F. Tables of results

Finally, we summarize our numerical results for constant baryon number sequences in Tables I – XII. In each table, we present the sequences by the orbital separation between the centers of masses of two stars normalized by the length

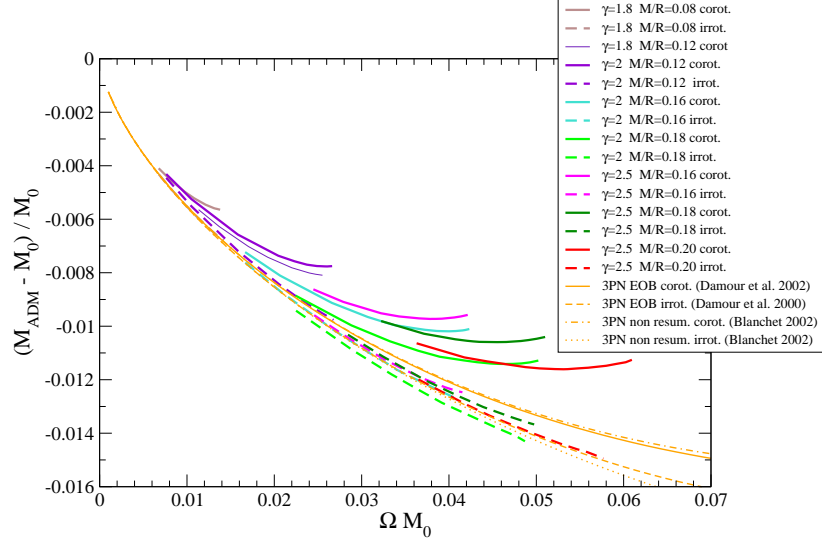


FIG. 26: Enlargement of Fig. 25 in the neutron star region, with some additional sequences.

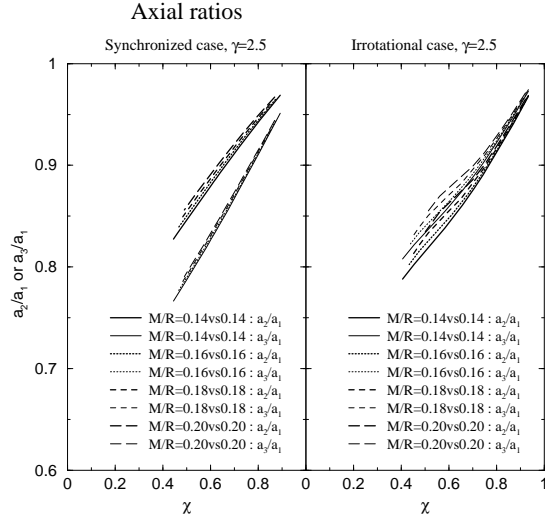


FIG. 27: Axial ratios  $a_2/a_1$  or  $a_3/a_1$  as a function of the cusp indicator  $\chi$  in the case of the adiabatic index  $\gamma = 2.5$ . The left (right) panel is for synchronized (irrotational) binaries. Solid, dotted, dashed, and long-dashed lines denote the cases of  $M/R = 0.14$  vs  $0.14$ ,  $0.16$  vs  $0.16$ ,  $0.18$  vs  $0.18$ , and  $0.20$  vs  $0.20$ , respectively. Thick and thin lines are the axial ratios  $a_2/a_1$  and  $a_3/a_1$ .

scale in polytropic units:

$$\bar{d}_G := \frac{d_G}{R_{\text{poly}}}, \quad (33)$$

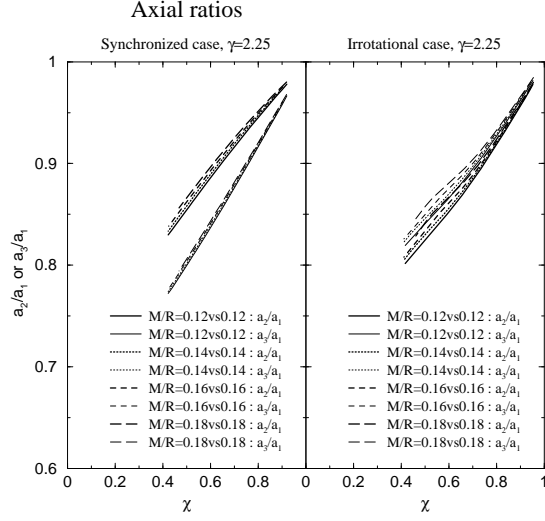


FIG. 28: Same as Fig. 27 but for  $\gamma = 2.25$ . Solid, dotted, dashed, and long-dashed lines denote the cases of  $M/R = 0.12$  vs  $0.12$ ,  $0.14$  vs  $0.14$ ,  $0.16$  vs  $0.16$ , and  $0.18$  vs  $0.18$ , respectively.

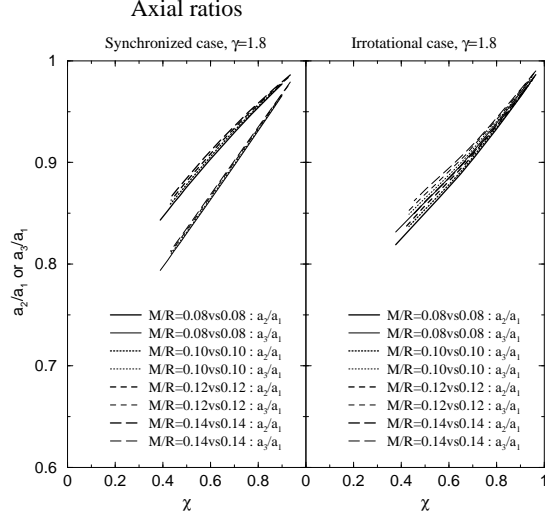


FIG. 29: Same as Fig. 27 but for  $\gamma = 1.8$ . Solid, dotted, dashed, and long-dashed lines denote the cases of  $M/R = 0.08$  vs  $0.08$ ,  $0.10$  vs  $0.10$ ,  $0.12$  vs  $0.12$ , and  $0.14$  vs  $0.14$ , respectively.

and also by the orbital separation between the two coordinate centers normalized by the summation of the radii of stars in the direction of its companion: <sup>5</sup>

$$\tilde{d} := \frac{d}{a_1 + a'_1}. \quad (34)$$

Here we define the length scale in polytropic units as

$$R_{\text{poly}} := \kappa^{1/2(\gamma-1)}, \quad (35)$$

---

<sup>5</sup> In Paper III, the equation (15) should be replaced by this equation.

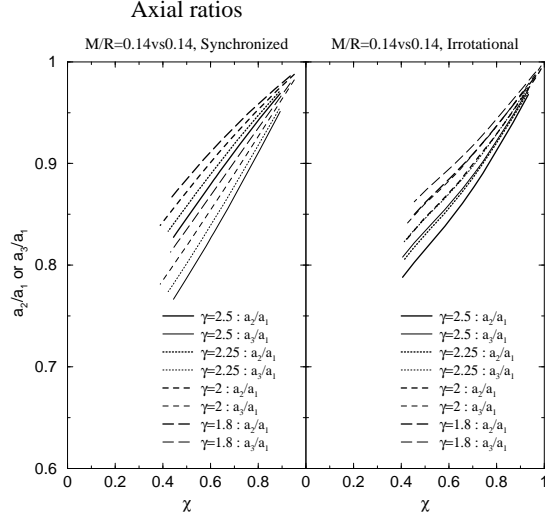


FIG. 30: Axial ratios as a function of the cusp indicator  $\chi$ . Left (right) is for synchronized (irrotational) binary systems with the compactness  $M/R = 0.14$  vs  $0.14$ . Solid, dotted, dashed, and long-dashed lines denote the cases of adiabatic indices  $\gamma = 2.5, 2.25, 2,$  and  $1.8$ , respectively. Thick and thin line are for the axial ratios  $a_2/a_1$  and  $a_3/a_1$ .

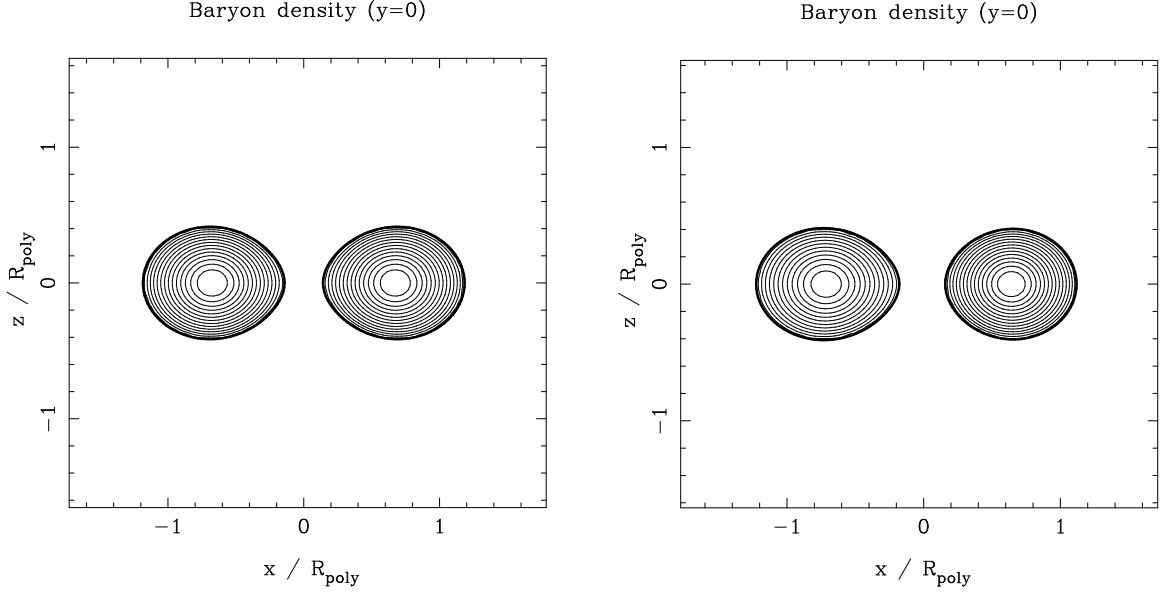


FIG. 31: Isocontours of the baryon density for synchronized binary systems with  $\gamma = 2.5$ . The left panel is for the compactness  $M/R = 0.16$  vs  $0.16$  and the orbital separation  $d_G/R_{\text{poly}} = 1.349$ , and the right panel  $M/R = 0.16$  vs  $0.18$  and  $d_G/R_{\text{poly}} = 1.356$ . The orbital axis is located on  $x = 0$  in each panel. The thick solid lines denote the surface of the stars.

by using the polytropic constant  $\kappa$  and the adiabatic index  $\gamma$ . In the tables, we also show the dimensionless orbital angular velocity:

$$\bar{\Omega} := \Omega \kappa^{1/2(\gamma-1)}, \quad (36)$$

the dimensionless ADM mass:

$$\bar{M} := M \kappa^{-1/2(\gamma-1)}, \quad (37)$$

the dimensionless baryon mass:

$$\bar{M}_B := M_B \kappa^{-1/2(\gamma-1)}, \quad (38)$$

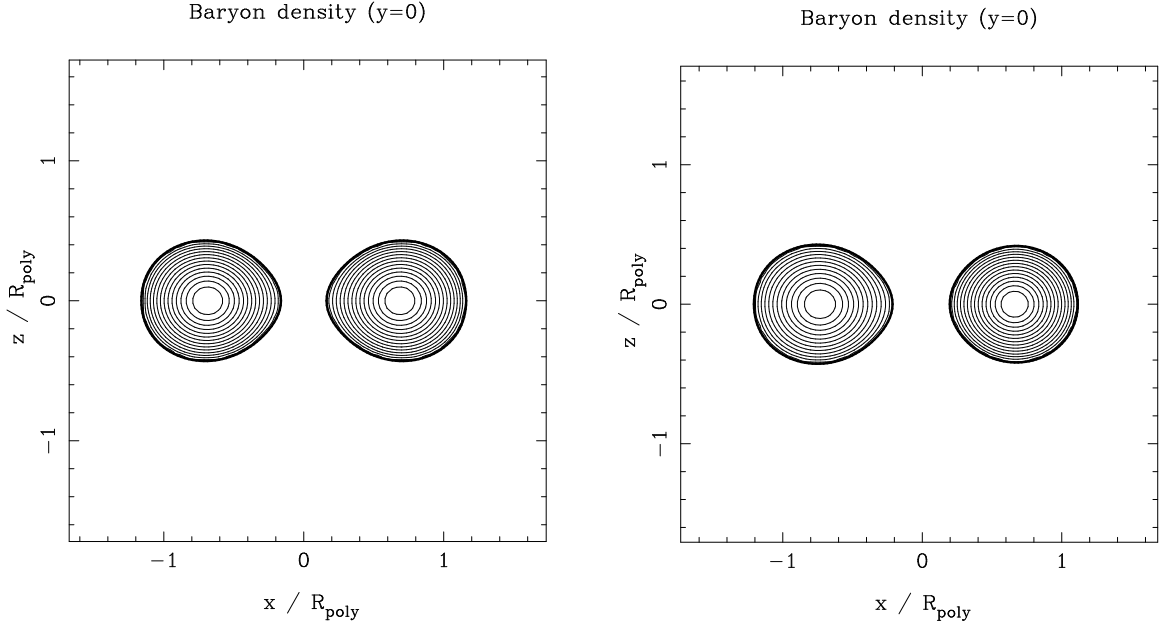


FIG. 32: Same as Fig. 31, but for irrotational binary systems. The left panel is for  $d_G/R_{\text{poly}} = 1.370$ , and the right for  $d_G/R_{\text{poly}} = 1.393$ .

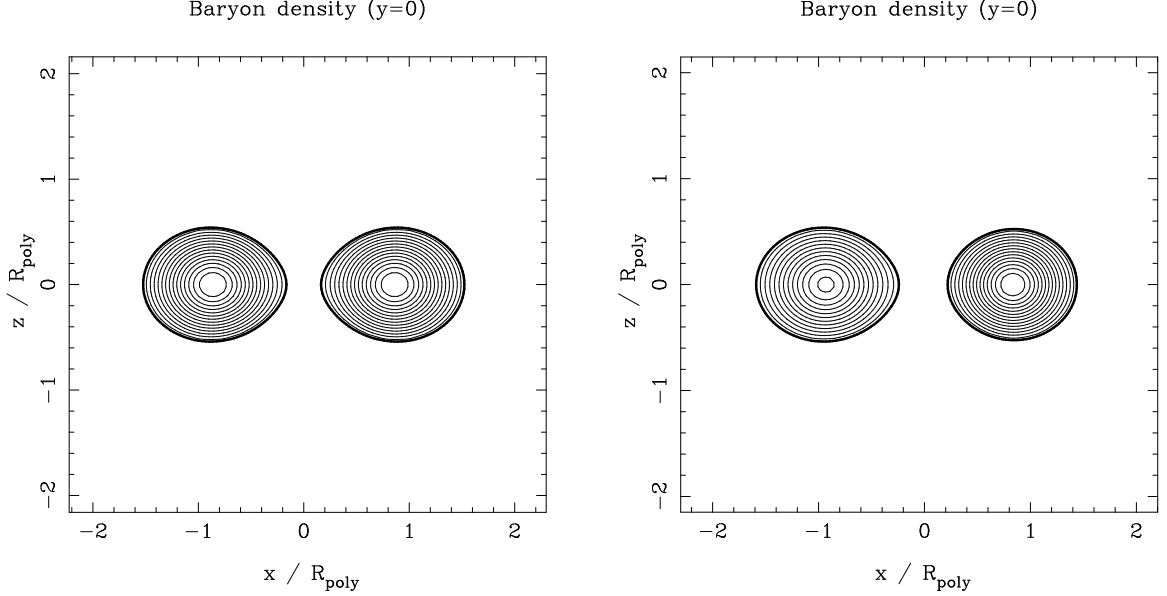


FIG. 33: Isocontours of the baryon density for synchronized binary systems with  $\gamma = 2.25$ . The left panel is for the compactness  $M/R = 0.14$  vs  $0.14$  and the orbital separation  $d_G/R_{\text{poly}} = 1.724$ , and the right panel  $M/R = 0.14$  vs  $0.16$  and  $d_G/R_{\text{poly}} = 1.765$ . The orbital axis is located on  $x = 0$  in each panel.

and the dimensionless total angular momentum:

$$\bar{J} := J\kappa^{-1/(\gamma-1)}. \quad (39)$$

The absolute values of the relative error in the virial theorem:  $|VE(M)|$ ,  $|VE(FUS)|$ , and  $|VE(GB)|$  are defined in Eqs. (28) – (30).  $\delta e_c$  is the relative change in central energy density defined as

$$\delta e_c := \frac{e_c - e_{c,\infty}}{e_{c,\infty}}, \quad (40)$$

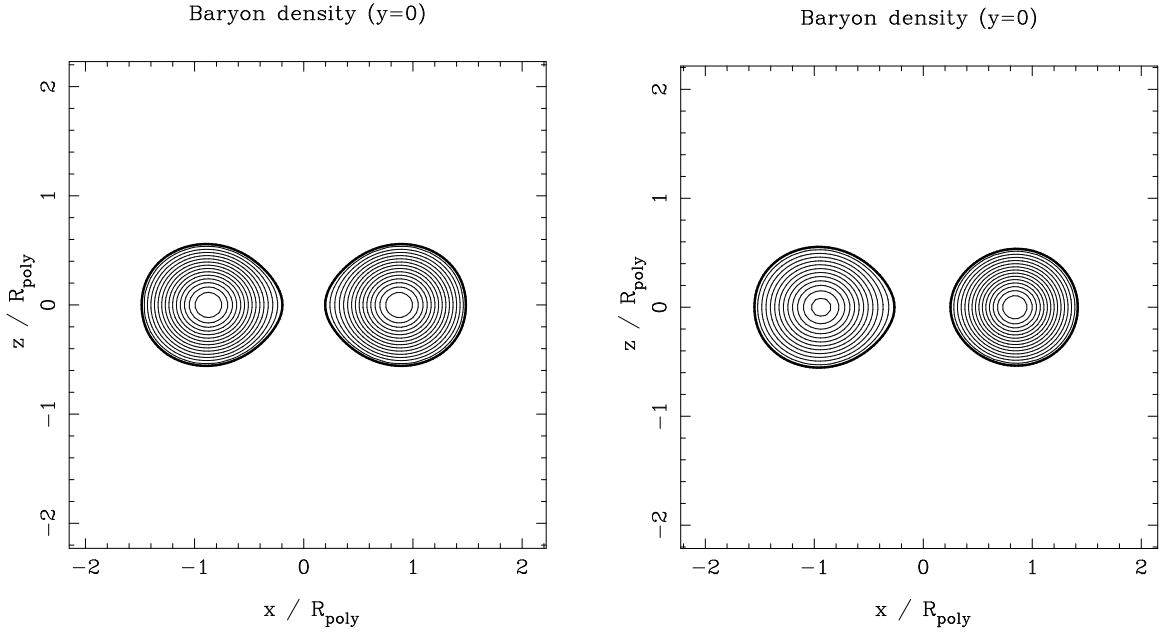


FIG. 34: Same as Fig. 33, but for irrotational binary systems. The left panel is for  $d_G/R_{\text{poly}} = 1.742$ , and the right for  $d_G/R_{\text{poly}} = 1.775$ .

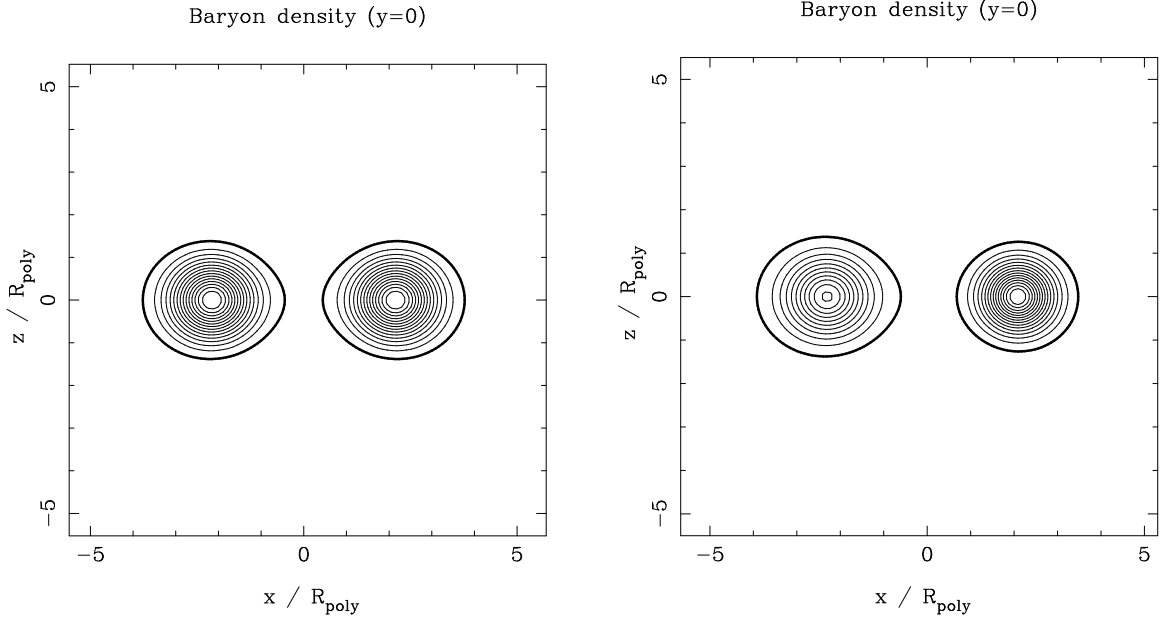


FIG. 35: Isocontours of the baryon density for synchronized binary systems with  $\gamma = 1.8$ . The left panel is for the compactness  $M/R = 0.10$  vs  $0.10$  and the orbital separation  $d_G/R_{\text{poly}} = 4.305$ , and the right panel  $M/R = 0.10$  vs  $0.12$  and  $d_G/R_{\text{poly}} = 4.391$ . The orbital axis is located on  $x = 0$  in each panel.

where  $e_c$  and  $e_{c,\infty}$  denote the central energy density and that of an isolated spherical star with the same baryon mass (or in other words, that of a star with an infinite separation from the companion star). In the tables, the prime denotes the values for the more massive star, and the symbol † denotes the turning point in the ADM mass (and the total angular momentum) along the sequence.

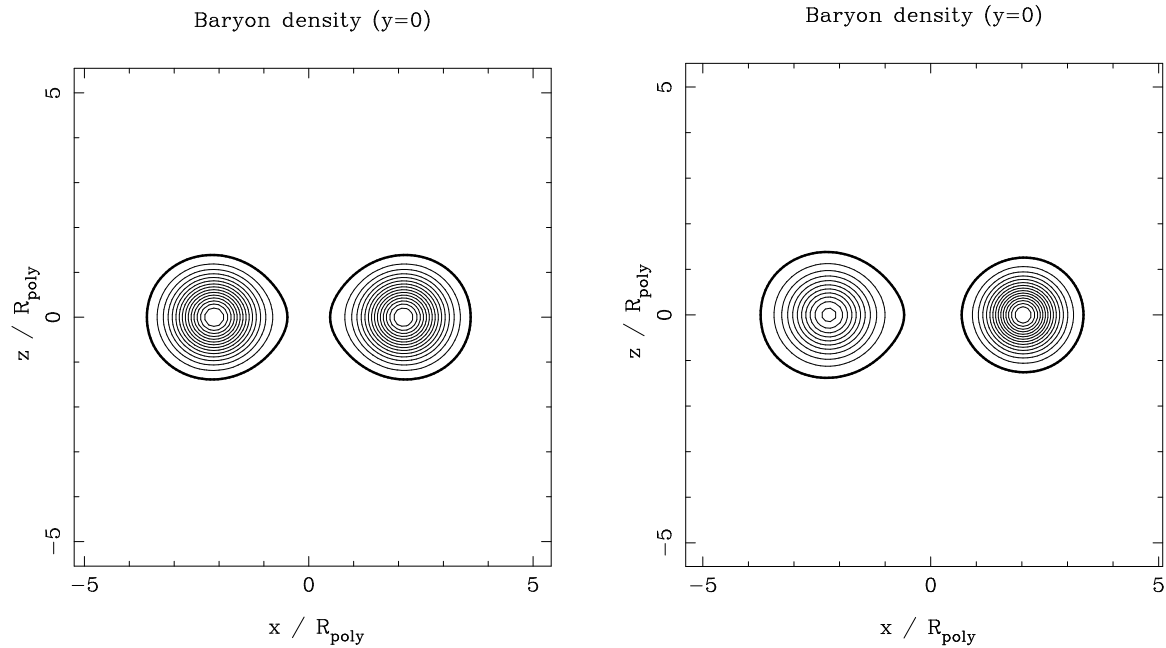


FIG. 36: Same as Fig. 35, but for irrotational binary systems. The left panel is for  $d_G/R_{\text{poly}} = 4.213$ , and the right for  $d_G/R_{\text{poly}} = 4.257$ .

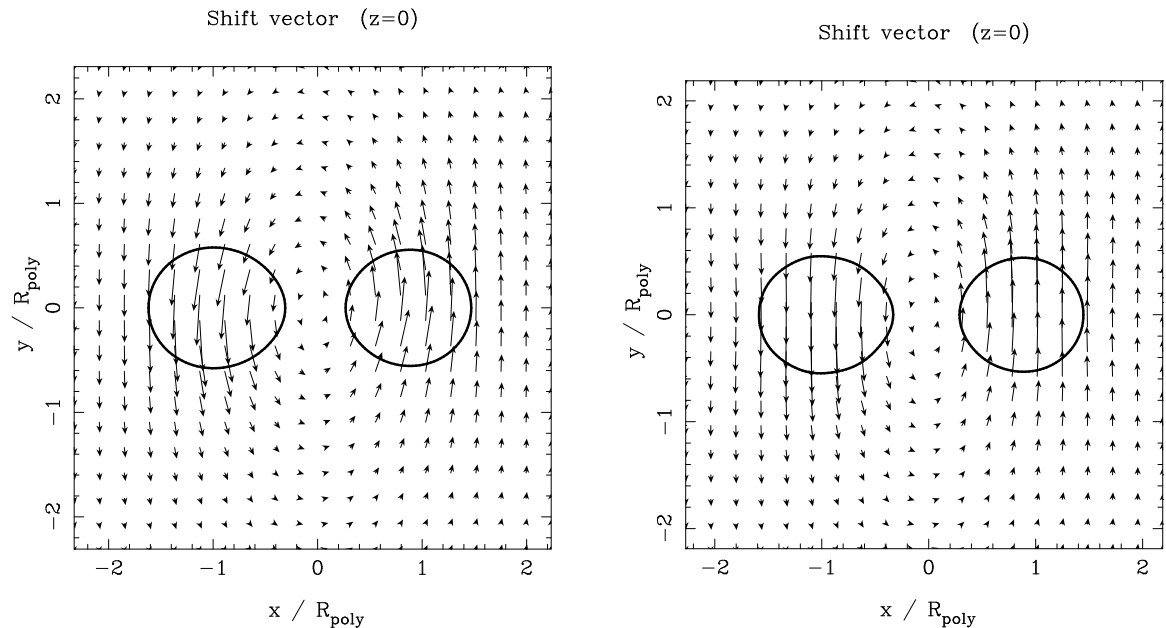


FIG. 37: Shift vector  $N^i$  of nonrotating coordinates in the orbital plane. Left (right) panel is for the synchronized (irrotational) binary system of the orbital separation  $d_G/R_{\text{poly}} = 1.846$  (1.843). These binary systems have the adiabatic index  $\gamma = 2.25$  and the compactness  $M/R = 0.14$  vs  $0.16$ . The thick solid lines denote the surface of the stars.

## V. DISCUSSION

As shown by Friedman et al. [44], the minimum (turning point) in the ADM mass in a constant baryon number sequence locates the appearance of a secular (resp. dynamical) instability for synchronized (resp. irrotational) binaries, thus defining the *innermost stable circular orbit (ISCO)*. The frequency at the ISCO is a potentially observable parameter by the gravitational wave detectors, and thus a very interesting quantity. The position of the ISCO for identical-mass binary systems is depicted as a function of the compactness parameter in Fig. 40. First of all, we have

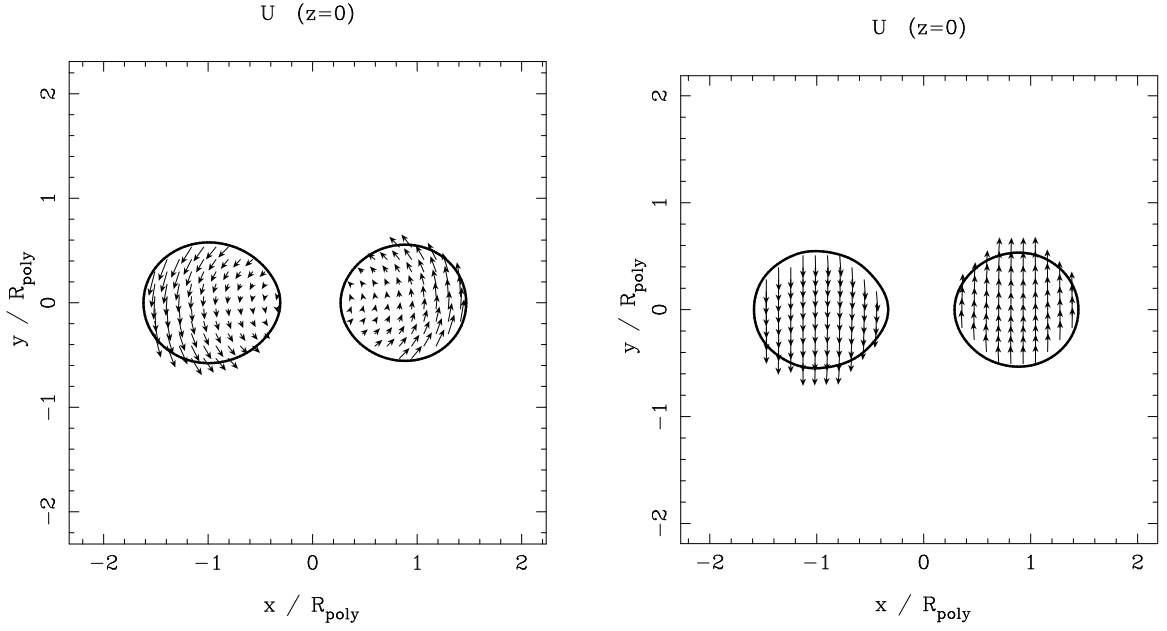


FIG. 38: Velocity field with respect to the Eulerian frame in the orbital plane. Left (right) panel is for the synchronized (irrotational) binary system of the orbital separation  $d_G/R_{\text{poly}} = 1.846$  (1.843). These binary systems have the adiabatic index  $\gamma = 2.25$  and the compactness  $M/R = 0.14$  vs  $0.16$ . The thick solid lines denote the surface of the stars.

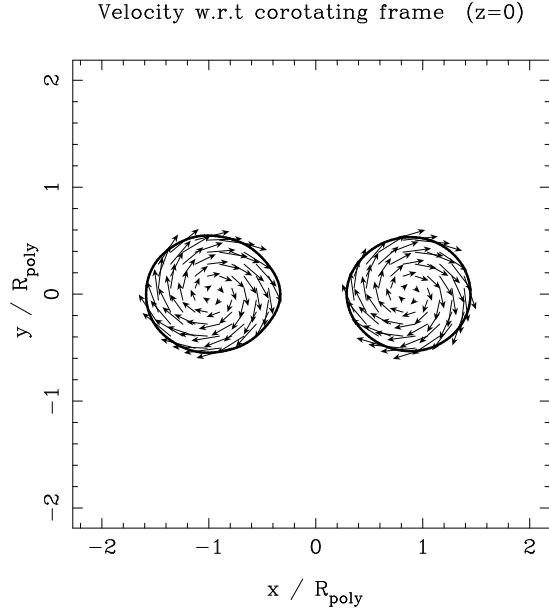


FIG. 39: Internal velocity field of the irrotational binary system with respect to the co-orbiting frame in the orbital plane when the separation  $d_G/R_{\text{poly}} = 1.843$ . The binary system has the adiabatic index  $\gamma = 2.25$  and the compactness  $M/R = 0.14$  vs  $0.16$ . The thick solid lines denote the surface of the stars.

to comment on the values of the Newtonian calculation. In this figure, the Newtonian results are shown as  $M/R = 0$ . For the irrotational binary systems, the values of  $\chi$  is slightly different from those in Paper II. This is because we have improved our numerical code to decrease the *aliasing error* which appears in the spectral method [70].

It is found and predicted several things from Fig. 40. Firstly, the turning points are found for synchronized binary systems for  $\gamma \geq 2$  and for irrotational ones for  $\gamma \geq 2.5$ . This last finding agrees with the results of Uryu et al. [37]. The turning point might exist for adiabatic index slightly lower than 2 for synchronized binary systems and 2.5 for

irrotational ones. However, since it is very difficult for our numerical code to calculate quasiequilibrium figures of  $\chi < 0.4$  for mildly relativistic cases and  $\chi < 0.5$  for highly relativistic ones, we cannot determine the exact value of the minimum adiabatic index which has the turning point. Secondly, the quantity  $\chi$  at the turning point increases proportionally to the compactness of the stars. This implies that the relative orbital separation at the turning point increases with the increase of the compactness. Thirdly, the inclination of lines for synchronized binary systems is larger than that for irrotational ones. Fourthly, we may assert that a turning point is found in Newtonian calculations for some value of the adiabatic index  $\gamma$ , it should exist in the general relativistic computations (within the IWM approximation) for the same value of  $\gamma$ , because the lines in Fig. 40 have a positive slope. It is worth to point out that even if the turning point is not found in the Newtonian sequences, the possibility to find it in the general relativistic computations does not vanish. In Fig. 40, some vertical lines which denote the maximum values of compactness for stable spherical stars are depicted. They show the limit of the existence of the turning point for each adiabatic index. Then, for an adiabatic index, the turning point could exist from a compactness  $M/R > 0$  to the maximum  $(M/R)_{\max}$  taking into account the fact that the line of the turning point has a positive inclination.

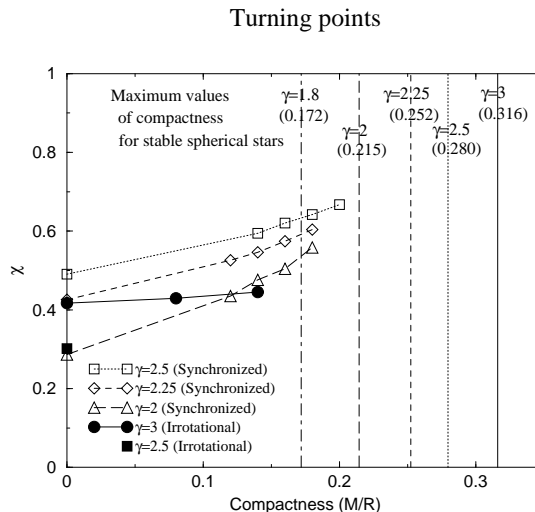


FIG. 40: Positions of the turning points of the ADM mass (and total angular momentum) in the sequence as a function of the compactness parameter. Solid line with filled circle is for the irrotational binary system with  $\gamma = 3$ . Dotted with open square, dashed with open diamond, and long-dashed with open triangle denote the results of synchronized binary systems with  $\gamma = 2.5, 2.25$ , and  $2$ , respectively. Vertical solid, dotted, dashed, and long-dashed lines are maximum values of compactness for stable spherical stars (at  $\chi = 1$ ) for  $\gamma = 3, 2.5, 2.25, 2$ , and  $1.8$ , respectively.

## VI. SUMMARY

We have developed a numerical code for obtaining quasiequilibrium sequences of binary neutron stars through the series of works [24, 25, 34, 35]. In the present article, we have presented the results of relativistic computations of both synchronized and irrotational rotation states, for polytropic equations of state with several adiabatic indices. We have considered not only binary systems composed of identical-mass stars but also different-mass systems. We have investigated the behaviors of various physical quantities along constant baryon number sequences (evolutionary sequences): the relative change in central energy density, the ADM mass, the total angular momentum, the axial ratios, the figures, as well as the location of the end point and that of the turning point in the ADM mass and angular momentum.

As one of interesting results, we propose, as a conjecture, that if the turning points defining the ISCO are found for the Newtonian calculations for some adiabatic index  $\gamma$ , they should exist in the general relativistic computations for the same value of  $\gamma$ .

## Acknowledgments

KT acknowledges a Grant-in-Aid for Scientific Research (No. 14-06898) of the Japanese Ministry of Education, Culture, Sports, Science and Technology.

- 
- [1] C. Cutler and K. S. Thorne, in *Proceedings of the 16th International Conference on General Relativity and Gravitation*, edited by N.T. Bishop and S.D. Maharaj (World Scientific, Singapore, 2002), preprint gr-qc/0204090.
- [2] R. Narayan, B. Paczynski, and T. Piran, *Astrophys. J. Lett.* **395**, L83 (1992).
- [3] H. Tagoshi et al, *Phys. Rev. D* **63**, 062001 (2001).
- [4] See for example, T. Tanaka and H. Tagoshi, *Phys. Rev. D* **62**, 082001 (2000).
- [5] T. W. Baumgarte and S. L. Shapiro, *Phys. Rep.* **376**, 41 (2003).
- [6] L. Blanchet, *Living Rev. Relativity* **5**, 3 (2002), <http://www.livingreviews.org/Articles/Volume5/2002-3blanchet/>
- [7] L. Blanchet, T. Damour, B. Iyer, C. M. Will, and A. G. Wiseman, *Phys. Rev. Lett.* **74**, 3515 (1995).
- [8] L. Blanchet, G. Faye, B. R. Iyer, and B. Joguet, *Phys. Rev. D* **65**, 061501 (2002).
- [9] M. Shibata, *Phys. Rev. D* **60**, 104052 (1999).
- [10] M. Shibata and K. Uryu, *Phys. Rev. D* **61**, 064001 (2000); *Prog. Theor. Phys.*, **107**, 265 (2002).
- [11] M. Shibata, K. Taniguchi, and K. Uryu, accepted to *Phys. Rev. D*.
- [12] K. Oohara and T. Nakamura, *Prog. Theor. Phys. Suppl.* **136**, 270 (1999).
- [13] M. Kawamura, K. Oohara, and T. Nakamura, submitted to *Prog. Theor. Phys.*, preprint astro-ph/0306481.
- [14] J. A. Font, T. Goodale, S. Iyer, M. Miller, L. Rezzolla, E. Seidel, N. Stergioulas, W.-M. Suen, and M. Tobias, *Phys. Rev. D* **65**, 084024 (2002).
- [15] M. D. Duez, P. Marronetti, S. L. Shapiro, and T. W. Baumgarte, *Phys. Rev. D* **67**, 024004 (2003).
- [16] J. A. Faber, P. Grandclément, F. A. Rasio, and K. Taniguchi, *Phys. Rev. Lett.* **89**, 231102 (2002).  
See also M. Saijo and T. Nakamura, *Phys. Rev. Lett.* **85**, 2665 (2000); *Phys. Rev. D* **63**, 064004 (2001), for a different idea to determine the radius of a neutron star.
- [17] M. Miller and W.-M. Suen, preprint gr-qc/0301112.
- [18] M. Miller, preprint gr-qc/0305024.
- [19] D. Lai, F. A. Rasio, and S. L. Shapiro, *Astrophys. J. Suppl. Ser.* **88**, 205 (1993); *Astrophys. J.* **420**, 811 (1994).
- [20] K. Taniguchi and T. Nakamura, *Phys. Rev. Lett.* **84**, 581 (2000); *Phys. Rev. D* **62**, 044040 (2000).
- [21] I. Hachisu and Y. Eriguchi, *Publ. Astron. Soc. Jpn.* **36**, 239 (1984).
- [22] I. Hachisu and Y. Eriguchi, *Publ. Astron. Soc. Jpn.* **36**, 259 (1984).
- [23] K. Uryu and Y. Eriguchi, *Astrophys. J. Suppl. Ser.* **118**, 563 (1998).
- [24] K. Taniguchi, E. Gourgoulhon, and S. Bonazzola, *Phys. Rev. D* **64**, 064012 (2001): Paper II.
- [25] K. Taniguchi and E. Gourgoulhon, *Phys. Rev. D* **65**, 044027 (2002).
- [26] J. C. Lombardi, F. A. Rasio, and S. L. Shapiro, *Phys. Rev. D* **56**, 3416 (1997).
- [27] K. Taniguchi and M. Shibata, *Phys. Rev. D* **56**, 798 (1997).
- [28] M. Shibata and K. Taniguchi, *Phys. Rev. D* **56**, 811 (1997).
- [29] K. Taniguchi, *Prog. Theor. Phys.* **101**, 283 (1999).
- [30] M. Shibata, *Prog. Theor. Phys.* **96**, 317 (1996); *Phys. Rev. D* **55**, 6019 (1997).
- [31] T. W. Baumgarte, G. B. Cook, M. A. Scheel, S. L. Shapiro, and S. A. Teukolsky, *Phys. Rev. Lett.* **79**, 1182 (1997); *Phys. Rev. D* **57**, 7299 (1998).
- [32] P. Marronetti, G. J. Mathews, and J. R. Wilson, *Phys. Rev. D* **58**, 107503 (1998); *ibid.* **60**, 087301 (1999).
- [33] S. Bonazzola, E. Gourgoulhon, and J.-A. Marck, *Phys. Rev. Lett.* **82**, 892 (1999).
- [34] E. Gourgoulhon, P. Grandclément, K. Taniguchi, J.-A. Marck, and S. Bonazzola, *Phys. Rev. D* **63**, 064029 (2001): Paper I.
- [35] K. Taniguchi and E. Gourgoulhon, *Phys. Rev. D* **66**, 104019 (2002): Paper III.
- [36] K. Uryu and Y. Eriguchi, *Phys. Rev. D* **61**, 124023 (2000).
- [37] K. Uryu, M. Shibata, and Y. Eriguchi, *Phys. Rev. D* **62**, 104015 (2000).
- [38] F. Usui, K. Uryu, and Y. Eriguchi, *Phys. Rev. D* **61**, 024039 (1999).
- [39] F. Usui and Y. Eriguchi, *Phys. Rev. D* **65**, 064030 (2002).
- [40] P. Marronetti and S. L. Shapiro, submitted to *Phys. Rev. D.*, preprint gr-qc/0306075.
- [41] J.A. Isenberg : *Waveless approximation theories of gravity*, preprint University of Maryland, unpublished (1978).
- [42] J. Isenberg and J. Nester, in *General Relativity and Gravitation*, edited by A. Held (Plenum, New York, 1980), Vol. 1.
- [43] J. R. Wilson and G. J. Mathews, in *Frontiers in numerical relativity*, edited by C. R. Evans, L. S. Finn and D. W. Hobill (Cambridge University Press, Cambridge, England, 1989).
- [44] J. L. Friedman, K. Uryu, and M. Shibata, *Phys. Rev. D* **65**, 064035 (2002).
- [45] M.D. Duez, T.W. Baumgarte, and S.L. Shapiro, *Phys. Rev. D* **63**, 084030 (2001).
- [46] M. Shibata and K. Uryu, *Phys. Rev. D* **64**, 104017 (2001).
- [47] C. S. Kochanek, *Astrophys. J.* **398**, 234 (1992).
- [48] L. Bildsten and C. Cutler, *Astrophys. J.* **400**, 175 (1992).

- [49] S. Bonazzola, E. Gourgoulhon, and J.-A. Marck, *Phys. Rev. D* **56**, 7740 (1997).
- [50] H. Asada, *Phys. Rev. D* **57**, 7292 (1998).
- [51] M. Shibata, *Phys. Rev. D* **58**, 024012 (1998).
- [52] S. A. Teukolsky, *Astrophys. J.* **504**, 442 (1998).
- [53] See, for example, P. Haensel, in *Final States of Stellar Evolution*, edited by J.-M. Hameury and C. Motch, EAS Publications Series (EDP Sciences, 2003), preprint astro-ph/0301073.
- [54] R. A. Hulse and J. H. Taylor, *Astrophys. J.* **195**, L51 (1975).
- [55] S. E. Thorsett and D. Chakrabarty, *Astrophys. J.* **512**, 288 (1999).
- [56] J. H. Taylor and J. M. Weisberg, *Astrophys. J.* **345**, 434 (1989).
- [57] I. H. Stairs, Z. Arzoumanian, F. Camilo, A. G. Lyne, D. J. Nice, J. H. Taylor, S. E. Thorsett, and A. Wolszczan, *Astrophys. J.* **505**, 352 (1998).
- [58] F. Limousin et al., in preparation.
- [59] See, for example, J. W. York, in *Sources of Gravitational Radiation*, edited by L. Smarr (Cambridge University Press, Cambridge, England, 1979).
- [60] G. B. Cook, *Living Rev. Rel.* **5**, 1 (2000).
- [61] S. Bonazzola, E. Gourgoulhon, and J.-A. Marck, *Phys. Rev. D* **58**, 104020 (1998).
- [62] S. Bonazzola, E. Gourgoulhon, and J.-A. Marck, *J. Comput. Appl. Math.* **109**, 433 (1999).
- [63] P. Grandclément, S. Bonazzola, E. Gourgoulhon and J.-A. Marck, *J. Comput. Phys.* **170**, 231 (2001).
- [64] <http://www.lorene.obspm.fr/>
- [65] E. Gourgoulhon and S. Bonazzola, *Class. Quantum Grav.* **11**, 443 (1994).
- [66] T. Damour, P. Jaranowski, and G. Schäfer, *Phys. Rev. D* **62**, 084011 (2000).
- [67] T. Damour, E. Gourgoulhon, and P. Grandclément, *Phys. Rev. D* **66**, 024007 (2002).
- [68] L. Blanchet, *Phys. Rev. D* **65**, 124009 (2002).
- [69] P. Grandclément, E. Gourgoulhon, and S. Bonazzola, *Phys. Rev. D* **65**, 044021 (2002).
- [70] C. Canuto, M. Y. Hussaini, A. Quarteroni, and T. A. Zang, in *Spectral Methods in Fluid Dynamics*, (Springer-Verlag, New York, USA, 1988).

TABLE I: Orbital angular velocity, ADM mass, total angular momentum, virial errors, axial ratios, relative change in central energy density, and the cusp indicator  $\chi$  along constant baryon number sequences of identical mass binaries in synchronized motion, for various compactness. The symbol † denotes the turning point of the sequences.

Identical mass stars, Synchronized case, $\gamma = 2.5$												
$\bar{d}_G$	$\bar{d}$	$\bar{\Omega}$	$\bar{M}$	$\bar{J}$	$ VE(M) $	$ VE(GB) $	$ VE(FUS) $	$a_2/a_1$	$a_3/a_1$	$\delta e_c$	$\chi$	
$M/R = 0.14$ vs $0.14$ , $\bar{M}_B = 0.08742$ vs. $0.08742$												
2.186	2.238	0.1126	0.1601	2.964(-2)	1.174(-5)	2.242(-5)	2.123(-5)	0.9689	0.9512	-1.397(-2)	0.8927	
1.822	1.829	0.1452	0.1599	2.857(-2)	8.314(-6)	1.627(-5)	1.529(-5)	0.9443	0.9134	-2.447(-2)	0.8072	
1.640	1.607	0.1681	0.1599	2.819(-2)	6.026(-6)	1.204(-5)	1.130(-5)	0.9187	0.8771	-3.453(-2)	0.7232	
1.531	1.461	0.1851	0.1599	2.806(-2)	3.095(-5)	5.471(-5)	5.052(-5)	0.8924	0.8426	-4.397(-2)	0.6408	
† 1.487	1.398	0.1928	0.1599	2.805(-2)	2.776(-5)	4.804(-5)	4.397(-5)	0.8774	0.8240	-4.897(-2)	0.5948	
1.458	1.352	0.1983	0.1599	2.806(-2)	2.640(-2)	4.414(-5)	4.020(-5)	0.8650	0.8091	-5.288(-2)	0.5573	
1.421	1.290	0.2056	0.1599	2.810(-2)	2.633(-5)	4.088(-5)	3.712(-5)	0.8454	0.7865	-5.864(-2)	0.4984	
1.395	1.242	0.2111	0.1599	2.815(-2)	2.766(-5)	4.321(-5)	4.045(-5)	0.8274	0.7665	-6.343(-2)	0.4445	
$M/R = 0.16$ vs $0.16$ , $\bar{M}_B = 0.1005$ vs. $0.1005$												
2.004	2.127	0.1336	0.1816	3.579(-2)	1.736(-5)	3.375(-5)	3.200(-5)	0.9647	0.9435	-1.840(-2)	0.8729	
1.822	1.916	0.1523	0.1815	3.519(-2)	1.450(-5)	2.846(-5)	2.689(-5)	0.9523	0.9238	-2.455(-2)	0.8279	
1.640	1.694	0.1759	0.1814	3.471(-2)	1.155(-5)	2.198(-5)	2.063(-5)	0.9316	0.8930	-3.417(-2)	0.7564	
1.495	1.500	0.1998	0.1814	3.450(-2)	5.189(-5)	9.531(-5)	8.895(-5)	0.9021	0.8527	-4.663(-2)	0.6603	
† 1.453	1.439	0.2077	0.1814	3.449(-2)	4.664(-5)	8.490(-5)	7.876(-5)	0.8894	0.8364	-5.156(-2)	0.6204	
1.422	1.392	0.2139	0.1814	3.450(-2)	4.221(-5)	7.586(-5)	6.990(-5)	0.8780	0.8222	-5.580(-2)	0.5849	
1.367	1.300	0.2258	0.1814	3.457(-2)	3.944(-5)	6.632(-5)	6.120(-5)	0.8510	0.7903	-6.496(-2)	0.5026	
1.349	1.265	0.2301	0.1814	3.462(-2)	4.404(-5)	6.957(-5)	6.392(-5)	0.8390	0.7767	-6.862(-2)	0.4663	
$M/R = 0.18$ vs $0.18$ , $\bar{M}_B = 0.1131$ vs. $0.1131$												
1.822	2.019	0.1582	0.2016	4.191(-2)	2.354(-5)	4.687(-5)	4.417(-5)	0.9599	0.9342	-2.481(-2)	0.8489	
1.640	1.794	0.1824	0.2016	4.133(-2)	1.872(-5)	3.723(-5)	3.505(-5)	0.9434	0.9084	-3.410(-2)	0.7885	
1.531	1.651	0.2000	0.2015	4.110(-2)	3.294(-5)	5.649(-5)	4.700(-5)	0.9277	0.8853	-4.231(-2)	0.7339	
1.459	1.551	0.2135	0.2015	4.100(-2)	3.069(-5)	5.196(-5)	4.248(-5)	0.9129	0.8648	-4.958(-2)	0.6845	
† 1.409	1.479	0.2235	0.2015	4.098(-2)	6.083(-5)	1.115(-4)	1.021(-4)	0.8999	0.8474	-5.568(-2)	0.6418	
1.368	1.414	0.2327	0.2015	4.100(-2)	5.309(-5)	9.712(-5)	8.790(-5)	0.8858	0.8292	-6.189(-2)	0.5967	
1.313	1.322	0.2458	0.2015	4.110(-2)	4.138(-5)	7.013(-5)	6.147(-5)	0.8605	0.7986	-7.200(-2)	0.5182	
1.295	1.287	0.2505	0.2015	4.116(-2)	4.174(-5)	6.643(-5)	5.739(-5)	0.8493	0.7857	-7.606(-2)	0.4840	
$M/R = 0.20$ vs $0.20$ , $\bar{M}_B = 0.1250$ vs. $0.1250$												
1.822	2.140	0.1632	0.2200	4.847(-2)	3.860(-5)	7.632(-5)	7.280(-5)	0.9670	0.9442	-2.554(-2)	0.8694	
1.568	1.814	0.1994	0.2199	4.760(-2)	5.257(-5)	9.409(-5)	8.084(-5)	0.9464	0.9110	-3.973(-2)	0.7906	
1.459	1.665	0.2192	0.2198	4.737(-2)	4.707(-5)	8.401(-5)	7.058(-5)	0.9310	0.8878	-4.949(-2)	0.7350	
1.422	1.613	0.2266	0.2198	4.733(-2)	4.499(-5)	8.008(-5)	6.666(-5)	0.9243	0.8780	-5.357(-2)	0.7113	
† 1.366	1.530	0.2389	0.2198	4.729(-2)	4.199(-5)	7.341(-5)	5.976(-5)	0.9114	0.8600	-6.098(-2)	0.6674	
1.313	1.448	0.2515	0.2198	4.733(-2)	7.023(-5)	1.310(-4)	1.182(-4)	0.8955	0.8389	-6.954(-2)	0.6149	
1.259	1.355	0.2658	0.2199	4.745(-2)	6.260(-5)	1.099(-4)	9.640(-5)	0.8727	0.8102	-8.066(-2)	0.5419	
1.229	1.299	0.2740	0.2199	4.756(-2)	6.800(-5)	1.030(-4)	9.569(-5)	0.8560	0.7904	-8.789(-2)	0.4901	

TABLE II: Same as Table I but for different mass binary systems. The prime denotes the values for the more massive star.

Different mass stars, Synchronized case, $\gamma = 2.5$											
$\bar{d}_G$	$\bar{d}$	$\bar{\Omega}$	$\bar{M}$	$\bar{J}$	$ VE(M) $	$ VE(GB) $	$ VE(FUS) $	$a_2/a_1$	$a_3/a_1$	$\delta e_c$	$\chi$
								$a'_2/a'_1$	$a'_3/a'_1$	$\delta e'_c$	$\chi'$
$M/R = 0.14$ vs $0.16$ , $\bar{M}_B = 0.08742$ vs. $0.1005$											
2.004	2.080	0.1305	0.1708	3.224(-2)	1.331(-5)	2.585(-5)	2.443(-5)	0.9535	0.9300	-1.939(-2)	0.8452
								0.9691	0.9480	-1.740(-2)	0.8833
1.822	1.870	0.1489	0.1707	3.170(-2)	1.120(-5)	2.191(-5)	2.066(-5)	0.9365	0.9051	-2.617(-2)	0.7888
								0.9581	0.9300	-2.318(-2)	0.8419
1.640	1.647	0.1721	0.1707	3.127(-2)	8.836(-6)	1.663(-5)	1.558(-5)	0.9072	0.8651	-3.711(-2)	0.6960
								0.9398	0.9017	-3.217(-2)	0.7763
1.531	1.500	0.1894	0.1706	3.113(-2)	3.528(-5)	6.227(-5)	5.704(-5)	0.8768	0.8267	-4.752(-2)	0.6040
								0.9218	0.8758	-4.031(-2)	0.7148
† 1.482	1.429	0.1981	0.1706	3.111(-2)	3.086(-5)	5.309(-5)	4.804(-5)	0.8567	0.8027	-5.387(-2)	0.5443
								0.9105	0.8604	-4.506(-2)	0.6775
1.440	1.362	0.2062	0.1706	3.112(-2)	2.918(-5)	4.788(-5)	4.367(-5)	0.8337	0.7764	-6.056(-2)	0.4767
								0.8984	0.8445	-4.989(-2)	0.6383
1.421	1.330	0.2100	0.1707	3.114(-2)	3.091(-5)	4.906(-5)	4.524(-5)	0.8209	0.7624	-6.395(-2)	0.4396
								0.8921	0.8365	-5.228(-2)	0.6181
$M/R = 0.16$ vs $0.18$ , $\bar{M}_B = 0.1005$ vs. $0.1131$											
2.004	2.179	0.1364	0.1917	3.904(-2)	2.247(-5)	4.390(-5)	4.177(-5)	0.9606	0.9393	-1.936(-2)	0.8634
								0.9732	0.9541	-1.793(-2)	0.8951
1.822	1.965	0.1554	0.1916	3.839(-2)	1.908(-5)	3.759(-5)	3.562(-5)	0.9468	0.9181	-2.585(-2)	0.8150
								0.9640	0.9385	-2.372(-2)	0.8588
1.640	1.740	0.1792	0.1915	3.787(-2)	1.493(-5)	2.948(-5)	2.783(-5)	0.9238	0.8859	-3.608(-2)	0.7380
								0.9491	0.9144	-3.256(-2)	0.8023
1.495	1.546	0.2032	0.1915	3.762(-2)	2.677(-5)	4.474(-5)	3.698(-5)	0.8908	0.8413	-4.943(-2)	0.6339
								0.9286	0.8838	-4.357(-2)	0.7295
† 1.437	1.461	0.2145	0.1915	3.760(-2)	5.030(-5)	9.113(-5)	8.363(-5)	0.8701	0.8156	-5.715(-2)	0.5705
								0.9165	0.8666	-4.967(-2)	0.6879
1.386	1.380	0.2253	0.1915	3.763(-2)	4.373(-5)	7.603(-5)	6.901(-5)	0.8447	0.7858	-6.571(-2)	0.4947
								0.9025	0.8479	-5.620(-2)	0.6415
1.356	1.329	0.2330	0.1915	3.768(-2)	4.533(-5)	7.403(-5)	6.775(-5)	0.8249	0.7637	-7.168(-2)	0.4364
								0.8924	0.8349	-6.062(-2)	0.6086
$M/R = 0.18$ vs $0.20$ , $\bar{M}_B = 0.1131$ vs. $0.1250$											
1.822	2.077	0.1608	0.2108	4.506(-2)	2.951(-5)	5.847(-5)	5.549(-5)	0.9561	0.9304	-2.583(-2)	0.8400
								0.9699	0.9471	-2.465(-2)	0.8763
1.640	1.848	0.1852	0.2107	4.445(-2)	4.642(-5)	8.175(-5)	7.062(-5)	0.9381	0.9029	-3.555(-2)	0.7760
								0.9578	0.9268	-3.349(-2)	0.8282
1.459	1.604	0.2164	0.2107	4.407(-2)	3.889(-5)	6.799(-5)	5.682(-5)	0.9050	0.8567	-5.182(-2)	0.6657
								0.9366	0.8935	-4.770(-2)	0.7485
† 1.389	1.502	0.2308	0.2107	4.403(-2)	5.752(-5)	1.047(-4)	9.380(-5)	0.8838	0.8294	-6.127(-2)	0.5987
								0.9238	0.8747	-5.560(-2)	0.7027
1.349	1.440	0.2399	0.2107	4.405(-2)	5.591(-5)	9.670(-5)	8.621(-5)	0.8672	0.8091	-6.800(-2)	0.5479
								0.9142	0.8613	-6.114(-2)	0.6695
1.313	1.378	0.2487	0.2107	4.411(-2)	5.155(-5)	8.475(-5)	7.485(-5)	0.8476	0.7860	-7.556(-2)	0.4883
								0.9035	0.8468	-6.699(-2)	0.6332
1.295	1.345	0.2534	0.2107	4.415(-2)	5.715(-5)	8.631(-5)	7.711(-5)	0.8354	0.7722	-7.967(-2)	0.4522
								0.8971	0.8384	-7.031(-2)	0.6120

TABLE III: Same as Table I but for irrotational binaries.

Identical mass stars, Irrotational case, $\gamma = 2.5$											
$\bar{d}_G$	$\bar{d}$	$\bar{\Omega}$	$\bar{M}$	$\bar{J}$	$ VE(M) $	$ VE(GB) $	$ VE(FUS) $	$a_2/a_1$	$a_3/a_1$	$\delta e_c$	$\chi$
$M/R = 0.14$ vs $0.14$ , $\bar{M}_B = 0.08742$ vs. $0.08742$											
2.185	2.266	0.1129	0.1600	2.765(-2)	1.044(-5)	1.994(-5)	1.865(-5)	0.9678	0.9729	-4.680(-4)	0.9344
1.821	1.865	0.1459	0.1598	2.599(-2)	6.162(-6)	1.208(-5)	1.095(-5)	0.9403	0.9474	-1.371(-3)	0.8693
1.565	1.552	0.1803	0.1596	2.487(-2)	1.366(-5)	2.090(-5)	1.565(-6)	0.8903	0.9018	-3.843(-3)	0.7422
1.491	1.446	0.1930	0.1595	2.458(-2)	2.819(-5)	5.056(-5)	4.520(-5)	0.8608	0.8751	-5.587(-3)	0.6573
1.454	1.383	0.1999	0.1595	2.445(-2)	2.273(-5)	4.210(-5)	3.612(-5)	0.8384	0.8548	-6.944(-3)	0.5839
1.436	1.346	0.2036	0.1595	2.439(-2)	1.021(-5)	2.298(-5)	1.561(-5)	0.8230	0.8407	-7.880(-3)	0.5286
1.417	1.302	0.2075	0.1595	2.434(-2)	1.346(-5)	1.706(-6)	1.353(-5)	0.8027	0.8219	-9.217(-3)	0.4548
1.406	1.272	0.2100	0.1595	2.432(-2)	4.416(-5)	3.417(-5)	5.155(-5)	0.7881	0.8079	-1.036(-2)	0.4062
$M/R = 0.16$ vs $0.16$ , $\bar{M}_B = 0.1005$ vs. $0.1005$											
2.003	2.159	0.1341	0.1814	3.313(-2)	1.458(-5)	2.834(-5)	2.643(-5)	0.9630	0.9688	-7.015(-4)	0.9216
1.821	1.952	0.1531	0.1813	3.215(-2)	1.132(-5)	2.204(-5)	2.023(-5)	0.9489	0.9557	-1.217(-3)	0.8873
1.638	1.735	0.1770	0.1811	3.119(-2)	6.595(-6)	1.327(-5)	1.170(-5)	0.9244	0.9332	-2.361(-3)	0.8262
1.492	1.541	0.2014	0.1810	3.048(-2)	1.761(-5)	2.864(-5)	2.062(-5)	0.8868	0.8992	-4.562(-3)	0.7261
1.455	1.486	0.2085	0.1810	3.031(-2)	4.860(-5)	9.070(-5)	8.259(-5)	0.8719	0.8857	-5.510(-3)	0.6815
1.418	1.424	0.2161	0.1809	3.016(-2)	3.861(-5)	7.434(-5)	6.531(-5)	0.8512	0.8669	-6.816(-3)	0.6118
1.381	1.341	0.2242	0.1809	3.003(-2)	2.983(-5)	1.013(-5)	3.139(-5)	0.8160	0.8343	-9.212(-3)	0.4776
1.370	1.311	0.2268	0.1809	2.999(-2)	9.006(-5)	8.473(-5)	1.159(-4)	0.8023	0.8212	-1.048(-2)	0.4336
$M/R = 0.18$ vs $0.18$ , $\bar{M}_B = 0.1131$ vs. $0.1131$											
2.003	2.268	0.1396	0.2015	3.957(-2)	2.342(-5)	4.589(-5)	4.303(-5)	0.9687	0.9744	-6.386(-4)	0.9336
1.638	1.836	0.1837	0.2012	3.738(-2)	1.217(-5)	2.452(-5)	2.199(-5)	0.9377	0.9457	-2.020(-3)	0.8558
1.529	1.695	0.2018	0.2011	3.676(-2)	2.773(-5)	4.855(-5)	3.709(-5)	0.9180	0.9278	-3.182(-3)	0.8051
1.456	1.595	0.2156	0.2010	3.636(-2)	2.364(-5)	4.107(-5)	2.932(-5)	0.8986	0.9103	-4.452(-3)	0.7522
1.382	1.480	0.2313	0.2009	3.601(-2)	5.059(-5)	9.859(-5)	8.570(-5)	0.8674	0.8821	-6.561(-3)	0.6514
1.345	1.395	0.2399	0.2009	3.583(-2)	6.626(-5)	6.451(-5)	9.658(-5)	0.8335	0.8505	-9.023(-3)	0.5141
1.327	1.347	0.2443	0.2009	3.574(-2)	2.324(-4)	2.930(-4)	3.523(-4)	0.8126	0.8305	-1.139(-2)	0.4510
1.308	1.298	0.2489	0.2008	3.565(-2)	4.501(-4)	5.946(-4)	6.889(-4)	0.7909	0.8094	-1.453(-2)	0.4008
$M/R = 0.20$ vs $0.20$ , $\bar{M}_B = 0.1250$ vs. $0.1250$											
1.821	2.178	0.1642	0.2197	4.471(-2)	3.029(-5)	6.026(-5)	5.617(-5)	0.9650	0.9712	-9.649(-4)	0.9219
1.565	1.860	0.2011	0.2194	4.304(-2)	1.725(-5)	3.517(-5)	3.136(-5)	0.9407	0.9487	-2.287(-3)	0.8590
1.383	1.608	0.2372	0.2192	4.196(-2)	2.926(-5)	5.391(-5)	3.697(-5)	0.9005	0.9124	-5.184(-3)	0.7493
1.346	1.549	0.2458	0.2191	4.177(-2)	2.349(-5)	4.314(-5)	2.574(-5)	0.8855	0.8989	-6.292(-3)	0.6993
1.328	1.512	0.2504	0.2191	4.168(-2)	3.678(-5)	8.046(-5)	5.968(-5)	0.8733	0.8877	-7.089(-3)	0.6457
1.309	1.464	0.2548	0.2191	4.155(-2)	9.508(-5)	1.215(-4)	1.618(-4)	0.8540	0.8697	-8.684(-3)	0.5621
1.291	1.417	0.2593	0.2191	4.141(-2)	3.268(-4)	4.764(-4)	5.496(-4)	0.8347	0.8515	-1.113(-2)	0.5015
1.272	1.370	0.2640	0.2190	4.126(-2)	6.048(-4)	8.985(-4)	1.013(-3)	0.8157	0.8334	-1.426(-2)	0.4565

TABLE IV: Same as Table III but for different mass binary systems. The prime denotes the values for the more massive star.

Different mass stars, Irrotational case, $\gamma = 2.5$											
$\bar{d}_G$	$\bar{d}$	$\bar{\Omega}$	$\bar{M}$	$\bar{J}$	$ VE(M) $	$ VE(GB) $	$ VE(FUS) $	$a_2/a_1$	$a_3/a_1$	$\delta e_c$	$\chi$
								$a'_2/a'_1$	$a'_3/a'_1$	$\delta e'_c$	$\chi'$
$M/R = 0.14$ vs $0.16$ , $\bar{M}_B = 0.08742$ vs. $0.1005$											
2.003	2.112	0.1309	0.1707	2.978(-2)	1.129(-5)	2.193(-5)	2.036(-5)	0.9509	0.9581	-1.012(-3)	0.8976
								0.9677	0.9725	-5.307(-4)	0.9307
1.821	1.906	0.1496	0.1705	2.888(-2)	8.442(-6)	1.665(-5)	1.521(-5)	0.9316	0.9402	-1.799(-3)	0.8516
								0.9553	0.9609	-9.288(-4)	0.9004
1.638	1.687	0.1732	0.1704	2.800(-2)	4.911(-6)	9.372(-6)	8.187(-6)	0.8967	0.9083	-3.597(-3)	0.7634
								0.9339	0.9411	-1.813(-3)	0.8466
1.528	1.540	0.1908	0.1703	2.751(-2)	1.560(-5)	2.468(-5)	1.816(-5)	0.8576	0.8730	-6.068(-3)	0.6577
								0.9116	0.9209	-2.942(-3)	0.7884
1.491	1.484	0.1974	0.1703	2.735(-2)	3.031(-5)	5.431(-5)	4.769(-5)	0.8372	0.8545	-7.402(-3)	0.5939
								0.9012	0.9115	-3.515(-3)	0.7598
1.455	1.420	0.2045	0.1702	2.721(-2)	1.747(-5)	3.441(-5)	2.640(-5)	0.8071	0.8270	-9.393(-3)	0.4892
								0.8881	0.8996	-4.267(-3)	0.7218
1.436	1.382	0.2082	0.1702	2.715(-2)	9.138(-7)	1.224(-5)	1.942(-5)	0.7863	0.8075	-1.095(-2)	0.4182
								0.8798	0.8922	-4.740(-3)	0.6966
$M/R = 0.16$ vs $0.18$ , $\bar{M}_B = 0.1005$ vs. $0.1131$											
1.821	2.002	0.1562	0.1913	3.515(-2)	1.487(-5)	2.951(-5)	2.721(-5)	0.9428	0.9508	-1.527(-3)	0.8751
								0.9618	0.9673	-8.614(-4)	0.9142
1.638	1.782	0.1805	0.1912	3.413(-2)	9.770(-6)	1.956(-5)	1.748(-5)	0.9153	0.9256	-2.943(-3)	0.8067
								0.9442	0.9510	-1.622(-3)	0.8697
1.565	1.688	0.1921	0.1911	3.374(-2)	2.498(-5)	4.281(-5)	3.331(-5)	0.8976	0.9096	-4.048(-3)	0.7612
								0.9333	0.9411	-2.188(-3)	0.8416
1.492	1.588	0.2051	0.1910	3.336(-2)	2.221(-5)	3.699(-5)	2.737(-5)	0.8726	0.8870	-5.704(-3)	0.6917
								0.9187	0.9278	-3.017(-3)	0.8028
1.455	1.534	0.2122	0.1910	3.319(-2)	2.025(-5)	3.301(-5)	2.328(-5)	0.8548	0.8710	-6.916(-3)	0.6365
								0.9092	0.9192	-3.593(-3)	0.7766
1.419	1.471	0.2198	0.1910	3.302(-2)	3.680(-5)	7.472(-5)	6.303(-5)	0.8280	0.8465	-8.712(-3)	0.5381
								0.8974	0.9085	-4.332(-3)	0.7425
1.393	1.417	0.2254	0.1909	3.291(-2)	2.161(-5)	6.228(-6)	2.607(-5)	0.7996	0.8197	-1.111(-2)	0.4382
								0.8867	0.8988	-5.015(-3)	0.7090
$M/R = 0.18$ vs $0.20$ , $\bar{M}_B = 0.1131$ vs. $0.1250$											
1.821	2.115	0.1617	0.2106	4.146(-2)	2.407(-5)	4.781(-5)	4.445(-5)	0.9530	0.9605	-1.310(-3)	0.8967
								0.9682	0.9735	-7.934(-4)	0.9281
1.565	1.798	0.1984	0.2103	3.987(-2)	3.436(-5)	6.119(-5)	4.780(-5)	0.9182	0.9287	-3.278(-3)	0.8090
								0.9456	0.9527	-1.931(-3)	0.8699
1.492	1.701	0.2115	0.2102	3.945(-2)	3.030(-5)	5.434(-5)	4.047(-5)	0.9003	0.9124	-4.498(-3)	0.7614
								0.9345	0.9426	-2.605(-3)	0.8405
1.419	1.596	0.2263	0.2101	3.904(-2)	2.503(-5)	4.469(-5)	3.043(-5)	0.8736	0.8884	-6.432(-3)	0.6828
								0.9191	0.9287	-3.631(-3)	0.7987
1.382	1.534	0.2343	0.2101	3.886(-2)	1.287(-5)	2.740(-5)	1.110(-5)	0.8507	0.8675	-8.001(-3)	0.5961
								0.9089	0.9194	-4.359(-3)	0.7693
1.364	1.497	0.2386	0.2100	3.876(-2)	1.977(-5)	1.155(-5)	3.520(-5)	0.8320	0.8501	-9.495(-3)	0.5208
								0.9026	0.9138	-4.810(-3)	0.7503
1.346	1.457	0.2429	0.2100	3.866(-2)	1.021(-4)	1.261(-4)	1.631(-4)	0.8119	0.8309	-1.178(-2)	0.4581
								0.8951	0.9070	-5.342(-3)	0.7258

TABLE V: Same as Table I but for  $\gamma = 2.25$ .

Identical mass stars, Synchronized case, $\gamma = 2.25$											
$\bar{d}_G$	$\bar{d}$	$\bar{\Omega}$	$\bar{M}$	$\bar{J}$	$ VE(M) $	$ VE(GB) $	$ VE(FUS) $	$a_2/a_1$	$a_3/a_1$	$\delta e_c$	$\chi$
$M/R = 0.12$ vs $0.12$ , $\bar{M}_B = 0.09316$ vs. $0.09316$											
2.925	2.304	0.07708	0.1734	3.724(-2)	8.099(-6)	1.407(-5)	1.317(-5)	0.9726	0.9578	-1.402(-2)	0.9002
2.701	2.113	0.08635	0.1733	3.646(-2)	7.249(-6)	1.259(-5)	1.174(-5)	0.9649	0.9457	-1.787(-2)	0.8712
2.251	1.714	0.1117	0.1732	3.510(-2)	4.990(-6)	8.736(-6)	8.072(-6)	0.9354	0.9019	-3.171(-2)	0.7650
2.026	1.492	0.1296	0.1731	3.462(-2)	2.062(-5)	3.400(-5)	3.093(-5)	0.9027	0.8580	-4.536(-2)	0.6549
1.936	1.392	0.1383	0.1731	3.452(-2)	1.853(-5)	2.870(-5)	2.572(-5)	0.8808	0.8307	-5.355(-2)	0.5840
† 1.881	1.327	0.1440	0.1731	3.450(-2)	1.659(-5)	2.505(-5)	2.232(-5)	0.8626	0.8091	-5.978(-2)	0.5263
1.845	1.278	0.1481	0.1731	3.451(-2)	1.695(-5)	2.373(-5)	2.153(-5)	0.8471	0.7912	-6.468(-2)	0.4773
1.813	1.231	0.1519	0.1731	3.455(-2)	1.961(-5)	2.624(-5)	2.560(-5)	0.8297	0.7721	-6.961(-2)	0.4231
$M/R = 0.14$ vs $0.14$ , $\bar{M}_B = 0.1080$ vs. $0.1080$											
2.701	2.229	0.09129	0.1985	4.535(-2)	1.297(-5)	2.327(-5)	2.192(-5)	0.9704	0.9535	-1.770(-2)	0.8879
2.251	1.821	0.1177	0.1983	4.366(-2)	9.395(-6)	1.688(-5)	1.573(-5)	0.9468	0.9171	-3.086(-2)	0.7986
2.026	1.600	0.1362	0.1982	4.302(-2)	7.380(-6)	1.267(-5)	1.170(-5)	0.9222	0.8820	-4.332(-2)	0.7109
1.936	1.505	0.1451	0.1982	4.285(-2)	3.392(-5)	5.874(-5)	5.399(-5)	0.9067	0.8611	-5.055(-2)	0.6580
1.846	1.402	0.1551	0.1982	4.275(-2)	2.858(-5)	4.793(-5)	4.339(-5)	0.8849	0.8336	-5.987(-2)	0.5862
† 1.808	1.354	0.1597	0.1982	4.274(-2)	2.765(-5)	4.403(-5)	3.958(-5)	0.8726	0.8186	-6.473(-2)	0.5464
1.756	1.284	0.1663	0.1982	4.277(-2)	2.930(-5)	4.107(-5)	3.686(-5)	0.8511	0.7936	-7.250(-2)	0.4779
1.724	1.235	0.1707	0.1982	4.283(-2)	3.209(-5)	4.785(-5)	4.456(-5)	0.8335	0.7740	-7.811(-2)	0.4228
$M/R = 0.16$ vs $0.16$ , $\bar{M}_B = 0.1219$ vs. $0.1219$											
2.701	2.364	0.09540	0.2215	5.416(-2)	2.248(-5)	4.136(-5)	3.929(-5)	0.9754	0.9609	-1.775(-2)	0.9039
2.251	1.943	0.1227	0.2213	5.214(-2)	1.703(-5)	3.126(-5)	2.936(-5)	0.9569	0.9309	-3.044(-2)	0.8295
2.026	1.720	0.1417	0.2211	5.134(-2)	1.374(-5)	2.462(-5)	2.291(-5)	0.9384	0.9029	-4.208(-2)	0.7592
1.936	1.625	0.1507	0.2211	5.110(-2)	2.577(-5)	4.027(-5)	3.303(-5)	0.9271	0.8867	-4.864(-2)	0.7185
1.801	1.474	0.1663	0.2211	5.086(-2)	5.052(-5)	9.016(-5)	8.315(-5)	0.9027	0.8536	-6.189(-2)	0.6334
† 1.736	1.394	0.1749	0.2211	5.082(-2)	4.393(-5)	7.597(-5)	6.912(-5)	0.8851	0.8313	-7.040(-2)	0.5746
1.666	1.298	0.1850	0.2211	5.088(-2)	4.497(-5)	6.625(-5)	5.946(-5)	0.8582	0.7992	-8.194(-2)	0.4876
1.630	1.241	0.1906	0.2211	5.097(-2)	5.881(-5)	8.377(-5)	7.738(-5)	0.8384	0.7769	-8.920(-2)	0.4250
$M/R = 0.18$ vs $0.18$ , $\bar{M}_B = 0.1347$ vs. $0.1347$											
2.701	2.522	0.09878	0.2419	6.251(-2)	3.691(-5)	6.915(-5)	6.619(-5)	0.9800	0.9677	-1.825(-2)	0.9190
2.251	2.084	0.1267	0.2416	6.018(-2)	2.898(-5)	5.451(-5)	5.162(-5)	0.9656	0.9434	-3.085(-2)	0.8576
2.026	1.854	0.1461	0.2415	5.922(-2)	2.451(-5)	4.556(-5)	4.254(-5)	0.9517	0.9211	-4.208(-2)	0.8011
1.891	1.709	0.1603	0.2414	5.878(-2)	3.901(-5)	6.457(-5)	5.406(-5)	0.9386	0.9011	-5.190(-2)	0.7505
1.712	1.502	0.1832	0.2414	5.842(-2)	7.229(-5)	1.321(-4)	1.219(-4)	0.9098	0.8605	-7.132(-2)	0.6458
† 1.662	1.439	0.1904	0.2414	5.839(-2)	6.523(-5)	1.173(-4)	1.074(-4)	0.8975	0.8445	-7.864(-2)	0.6036
1.577	1.320	0.2043	0.2414	5.849(-2)	5.633(-5)	9.448(-5)	8.565(-5)	0.8673	0.8072	-9.472(-2)	0.5033
1.554	1.284	0.2082	0.2414	5.855(-2)	6.519(-5)	1.036(-4)	9.563(-5)	0.8562	0.7943	-9.980(-2)	0.4677

TABLE VI: Same as Table V but for different mass binary systems. The prime denotes the values for the more massive star.

Different mass stars, Synchronized case, $\gamma = 2.25$												
$\bar{d}_G$	$\bar{d}$	$\bar{\Omega}$	$\bar{M}$	$\bar{J}$	$ VE(M) $	$ VE(GB) $	$ VE(FUS) $	$a_2/a_1$	$a_3/a_1$	$\delta e_c$	$\chi$	
								$a'_2/a'_1$	$a'_3/a'_1$	$\delta e'_c$	$\chi'$	
$M/R = 0.12$ vs $0.14$ , $\bar{M}_B = 0.09316$ vs. $0.1080$												
2.701	2.169	0.08889	0.1859	4.063(-2)	9.821(-6)	1.738(-5)	1.630(-5)	0.9595	0.9400	-1.916(-2)	0.8577	
								0.9744	0.9576	-1.665(-2)	0.8980	
2.476	1.970	0.1005	0.1858	3.983(-2)	8.511(-6)	1.508(-5)	1.407(-5)	0.9464	0.9208	-2.513(-2)	0.8113	
								0.9663	0.9443	-2.161(-2)	0.8655	
2.251	1.763	0.1148	0.1858	3.912(-2)	7.046(-6)	1.249(-5)	1.160(-5)	0.9254	0.8914	-3.421(-2)	0.7396	
								0.9538	0.9245	-2.894(-2)	0.8167	
2.026	1.539	0.1330	0.1857	3.858(-2)	1.413(-5)	1.996(-5)	1.610(-5)	0.8872	0.8419	-4.929(-2)	0.6154	
								0.9322	0.8925	-4.051(-2)	0.7370	
1.936	1.440	0.1418	0.1857	3.845(-2)	2.219(-5)	3.581(-5)	3.212(-5)	0.8610	0.8105	-5.851(-2)	0.5336	
								0.9187	0.8737	-4.719(-2)	0.6889	
1.891	1.385	0.1466	0.1857	3.842(-2)	2.220(-5)	3.382(-5)	3.011(-5)	0.8430	0.7899	-6.427(-2)	0.4782	
								0.9100	0.8621	-5.120(-2)	0.6590	
† 1.866	1.353	0.1494	0.1857	3.841(-2)	2.148(-5)	3.200(-5)	2.882(-5)	0.8308	0.7763	-6.788(-2)	0.4410	
								0.9045	0.8549	-5.365(-2)	0.6401	
$M/R = 0.14$ vs $0.16$ , $\bar{M}_B = 0.1080$ vs. $0.1219$												
2.476	2.090	0.1054	0.2099	4.857(-2)	1.519(-5)	2.769(-5)	2.606(-5)	0.9564	0.9340	-2.429(-2)	0.8402	
								0.9716	0.9524	-2.183(-2)	0.8829	
2.251	1.879	0.1203	0.2098	4.769(-2)	1.287(-5)	2.347(-5)	2.200(-5)	0.9404	0.9103	-3.265(-2)	0.7821	
								0.9615	0.9358	-2.899(-2)	0.8415	
2.026	1.655	0.1390	0.2097	4.698(-2)	9.989(-6)	1.804(-5)	1.681(-5)	0.9128	0.8721	-4.600(-2)	0.6867	
								0.9449	0.9097	-4.003(-2)	0.7761	
1.891	1.509	0.1529	0.2097	4.671(-2)	4.124(-5)	7.177(-5)	6.596(-5)	0.8840	0.8353	-5.852(-2)	0.5926	
								0.9285	0.8858	-4.988(-2)	0.7155	
1.846	1.457	0.1580	0.2097	4.665(-2)	3.974(-5)	6.562(-5)	5.982(-5)	0.8704	0.8188	-6.391(-2)	0.5494	
								0.9212	0.8756	-5.397(-2)	0.6893	
† 1.790	1.386	0.1649	0.2097	4.662(-2)	4.089(-5)	5.949(-5)	5.379(-5)	0.8485	0.7932	-7.193(-2)	0.4807	
								0.9101	0.8606	-5.989(-2)	0.6502	
1.765	1.353	0.1682	0.2097	4.662(-2)	3.651(-5)	5.655(-5)	5.304(-5)	0.8361	0.7793	-7.610(-2)	0.4425	
								0.9043	0.8530	-6.290(-2)	0.6300	
$M/R = 0.16$ vs $0.18$ , $\bar{M}_B = 0.1219$ vs. $0.1347$												
2.251	2.010	0.1248	0.2314	5.600(-2)	2.279(-5)	4.251(-5)	4.018(-5)	0.9528	0.9266	-3.174(-2)	0.8189	
								0.9687	0.9465	-2.973(-2)	0.8655	
2.026	1.783	0.1440	0.2313	5.514(-2)	3.483(-5)	5.659(-5)	4.793(-5)	0.9324	0.8966	-4.399(-2)	0.7440	
								0.9558	0.9253	-4.055(-2)	0.8120	
1.891	1.638	0.1580	0.2313	5.474(-2)	3.189(-5)	5.143(-5)	4.267(-5)	0.9126	0.8693	-5.496(-2)	0.6747	
								0.9437	0.9065	-4.995(-2)	0.7641	
1.801	1.536	0.1687	0.2312	5.456(-2)	3.025(-5)	4.807(-5)	3.943(-5)	0.8933	0.8441	-6.480(-2)	0.6098	
								0.9325	0.8899	-5.812(-2)	0.7212	
† 1.709	1.421	0.1811	0.2312	5.448(-2)	4.422(-5)	7.306(-5)	6.528(-5)	0.8638	0.8081	-7.820(-2)	0.5146	
								0.9165	0.8674	-6.886(-2)	0.6626	
1.689	1.394	0.1840	0.2312	5.449(-2)	4.380(-5)	7.051(-5)	6.284(-5)	0.8551	0.7980	-8.179(-2)	0.4871	
								0.9121	0.8614	-7.165(-2)	0.6468	
1.666	1.362	0.1874	0.2312	5.450(-2)	4.438(-5)	6.860(-5)	6.099(-5)	0.8440	0.7852	-8.614(-2)	0.4523	
								0.9067	0.8542	-7.496(-2)	0.6277	

TABLE VII: Same as Table V but for irrotational binaries.

Identical mass stars, Irrotational case, $\gamma = 2.25$											
$\bar{d}_G$	$\bar{d}$	$\bar{\Omega}$	$\bar{M}$	$\bar{J}$	$ VE(M) $	$ VE(GB) $	$ VE(FUS) $	$a_2/a_1$	$a_3/a_1$	$\delta e_c$	$\chi$
$M/R = 0.12$ vs $0.12$ , $\bar{M}_B = 0.09316$ vs. $0.09316$											
2.924	2.331	0.07722	0.1733	3.503(-2)	7.443(-6)	1.278(-5)	1.184(-5)	0.9720	0.9764	-3.975(-4)	0.9392
2.699	2.145	0.08654	0.1732	3.399(-2)	6.429(-6)	1.096(-6)	1.004(-5)	0.9639	0.9689	-6.208(-4)	0.9189
2.249	1.756	0.1121	0.1730	3.186(-2)	3.645(-6)	5.956(-6)	5.181(-6)	0.9318	0.9390	-1.880(-3)	0.8364
2.023	1.540	0.1302	0.1729	3.081(-2)	1.034(-5)	1.390(-5)	1.027(-5)	0.8949	0.9051	-3.891(-3)	0.7350
1.933	1.440	0.1390	0.1728	3.041(-2)	1.791(-5)	2.913(-5)	2.545(-5)	0.8689	0.8813	-5.503(-3)	0.6559
1.887	1.384	0.1438	0.1728	3.023(-2)	1.578(-5)	2.575(-5)	2.189(-5)	0.8500	0.8640	-6.695(-3)	0.5929
1.842	1.315	0.1490	0.1728	3.006(-2)	8.452(-6)	1.842(-5)	1.320(-5)	0.8223	0.8385	-8.430(-3)	0.4915
1.818	1.272	0.1518	0.1728	2.998(-2)	7.529(-6)	4.168(-6)	4.072(-6)	0.8017	0.8194	-9.802(-3)	0.4169
$M/R = 0.14$ vs $0.14$ , $\bar{M}_B = 0.1080$ vs. $0.1080$											
2.699	2.260	0.09153	0.1984	4.244(-2)	1.166(-5)	2.069(-5)	1.923(-5)	0.9696	0.9746	-5.469(-4)	0.9320
2.249	1.863	0.1182	0.1981	3.989(-2)	7.237(-6)	1.255(-5)	1.123(-5)	0.9440	0.9507	-1.557(-3)	0.8653
1.933	1.555	0.1460	0.1979	3.813(-2)	1.479(-5)	2.111(-5)	1.534(-5)	0.8979	0.9084	-4.220(-3)	0.7377
1.843	1.451	0.1562	0.1978	3.767(-2)	2.958(-5)	5.118(-5)	4.526(-5)	0.8710	0.8838	-6.024(-3)	0.6533
1.797	1.390	0.1617	0.1978	3.745(-2)	2.347(-5)	4.246(-5)	3.576(-5)	0.8502	0.8647	-7.406(-3)	0.5789
1.774	1.353	0.1647	0.1977	3.735(-2)	1.372(-5)	3.164(-5)	2.314(-5)	0.8352	0.8509	-8.379(-3)	0.5209
1.752	1.309	0.1677	0.1977	3.726(-2)	1.877(-5)	2.257(-6)	1.639(-5)	0.8148	0.8320	-9.855(-3)	0.4447
1.742	1.289	0.1690	0.1977	3.722(-2)	4.311(-5)	2.740(-5)	4.625(-5)	0.8052	0.8229	-1.068(-2)	0.4127
$M/R = 0.16$ vs $0.16$ , $\bar{M}_B = 0.1219$ vs. $0.1219$											
2.699	2.396	0.09567	0.2213	5.089(-2)	1.986(-5)	3.624(-5)	3.404(-5)	0.9749	0.9799	-4.866(-4)	0.9442
2.249	1.985	0.1232	0.2210	4.795(-2)	1.381(-5)	2.503(-5)	2.292(-5)	0.9548	0.9611	-1.302(-3)	0.8911
2.024	1.769	0.1425	0.2208	4.649(-2)	9.182(-6)	1.624(-5)	1.431(-5)	0.9339	0.9418	-2.449(-3)	0.8342
1.934	1.677	0.1518	0.2207	4.592(-2)	2.305(-5)	3.618(-5)	2.759(-5)	0.9208	0.9297	-3.308(-3)	0.7978
1.843	1.580	0.1620	0.2206	4.536(-2)	2.066(-5)	3.166(-5)	2.288(-5)	0.9030	0.9134	-4.559(-3)	0.7458
1.753	1.472	0.1737	0.2206	4.483(-2)	4.918(-5)	8.947(-5)	8.036(-5)	0.8757	0.8885	-6.554(-3)	0.6574
1.707	1.404	0.1800	0.2205	4.459(-2)	2.734(-5)	5.954(-5)	4.726(-5)	0.8515	0.8664	-8.228(-3)	0.5623
1.662	1.307	0.1868	0.2205	4.434(-2)	1.526(-4)	1.638(-4)	2.070(-4)	0.8080	0.8257	-1.237(-2)	0.4113
$M/R = 0.18$ vs $0.18$ , $\bar{M}_B = 0.1347$ vs. $0.1347$											
2.699	2.554	0.09906	0.2417	5.897(-2)	3.207(-5)	5.974(-5)	5.656(-5)	0.9798	0.9846	-4.427(-4)	0.9555
2.249	2.126	0.1274	0.2413	5.570(-2)	2.405(-5)	4.480(-5)	4.156(-5)	0.9643	0.9702	-1.115(-3)	0.9137
1.889	1.765	0.1614	0.2410	5.310(-2)	1.304(-5)	2.334(-5)	2.046(-5)	0.9337	0.9419	-3.042(-3)	0.8284
1.708	1.562	0.1849	0.2408	5.189(-2)	2.551(-5)	4.151(-5)	2.837(-5)	0.8982	0.9095	-5.944(-3)	0.7225
1.663	1.502	0.1918	0.2407	5.161(-2)	5.802(-5)	1.087(-4)	9.491(-5)	0.8826	0.8952	-7.211(-3)	0.6665
1.640	1.467	0.1953	0.2407	5.147(-2)	4.481(-5)	8.930(-5)	7.347(-5)	0.8704	0.8841	-8.092(-3)	0.6150
1.618	1.420	0.1989	0.2407	5.132(-2)	4.391(-5)	3.902(-5)	6.787(-5)	0.8509	0.8661	-9.735(-3)	0.5322
1.595	1.369	0.2026	0.2406	5.113(-2)	2.193(-4)	2.871(-4)	3.426(-4)	0.8288	0.8456	-1.248(-2)	0.4615

TABLE VIII: Same as Table VII but for different mass binary systems. The prime denotes the values for the more massive star.

Different mass stars, Irrotational case, $\gamma = 2.25$												
$\bar{d}_G$	$\bar{d}$	$\bar{\Omega}$	$\bar{M}$	$\bar{J}$	$ VE(M) $	$ VE(GB) $	$ VE(FUS) $	$a_2/a_1$	$a_3/a_1$	$\delta e_c$	$\chi$	
								$a'_2/a'_1$	$a'_3/a'_1$	$\delta e'_c$	$\chi'$	
$M/R = 0.12$ vs $0.14$ , $\bar{M}_B = 0.09316$ vs. $0.1080$												
2.699	2.200	0.08910	0.1858	3.794(-2)	8.995(-6)	1.576(-5)	1.458(-5)	0.9582	0.9643	-8.350(-4)	0.9072	
								0.9737	0.9778	-4.042(-4)	0.9404	
2.474	2.006	0.1008	0.1857	3.678(-2)	7.210(-6)	1.246(-5)	1.134(-5)	0.9440	0.9512	-1.386(-3)	0.8716	
								0.9651	0.9697	-6.597(-4)	0.9182	
2.249	1.805	0.1152	0.1856	3.561(-2)	5.310(-6)	8.974(-6)	7.943(-6)	0.9210	0.9298	-2.511(-3)	0.8119	
								0.9515	0.9570	-1.166(-3)	0.8822	
2.023	1.587	0.1337	0.1854	3.447(-2)	1.322(-5)	1.850(-5)	1.394(-5)	0.8772	0.8896	-5.215(-3)	0.6903	
								0.9273	0.9346	-2.322(-3)	0.8165	
1.933	1.487	0.1427	0.1854	3.403(-2)	2.179(-5)	3.612(-5)	3.144(-5)	0.8447	0.8598	-7.435(-3)	0.5874	
								0.9117	0.9203	-3.193(-3)	0.7718	
1.887	1.429	0.1476	0.1853	3.382(-2)	1.794(-5)	3.037(-5)	2.523(-5)	0.8190	0.8363	-9.171(-3)	0.4967	
								0.9014	0.9108	-3.804(-3)	0.7411	
1.865	1.395	0.1501	0.1853	3.373(-2)	1.079(-5)	2.103(-5)	1.498(-5)	0.8010	0.8196	-1.042(-2)	0.4320	
								0.8953	0.9052	-4.177(-3)	0.7220	
$M/R = 0.14$ vs $0.16$ , $\bar{M}_B = 0.1080$ vs. $0.1219$												
2.474	2.126	0.1058	0.2097	4.508(-2)	1.322(-5)	2.378(-5)	2.199(-5)	0.9546	0.9613	-1.128(-3)	0.8959	
								0.9707	0.9753	-5.989(-4)	0.9314	
2.249	1.921	0.1208	0.2096	4.371(-2)	1.029(-5)	1.834(-5)	1.665(-5)	0.9370	0.9449	-1.971(-3)	0.8498	
								0.9598	0.9651	-1.026(-3)	0.9020	
2.024	1.704	0.1398	0.2094	4.235(-2)	6.653(-6)	1.100(-5)	9.575(-6)	0.9055	0.9158	-3.843(-3)	0.7620	
								0.9411	0.9477	-1.950(-3)	0.8509	
1.888	1.560	0.1539	0.2093	4.156(-2)	1.779(-5)	2.613(-5)	1.900(-5)	0.8706	0.8841	-6.333(-3)	0.6606	
								0.9221	0.9303	-3.088(-3)	0.7974	
1.843	1.506	0.1592	0.2092	4.132(-2)	3.381(-5)	5.868(-5)	5.142(-5)	0.8523	0.8674	-7.640(-3)	0.5990	
								0.9135	0.9224	-3.646(-3)	0.7720	
1.797	1.444	0.1648	0.2092	4.108(-2)	2.288(-5)	4.357(-5)	3.482(-5)	0.8245	0.8418	-9.591(-3)	0.4945	
								0.9028	0.9126	-4.365(-3)	0.7394	
1.775	1.407	0.1678	0.2092	4.097(-2)	1.923(-6)	1.354(-5)	1.255(-6)	0.8037	0.8225	-1.127(-2)	0.4210	
								0.8963	0.9066	-4.813(-3)	0.7184	
$M/R = 0.16$ vs $0.18$ , $\bar{M}_B = 0.1219$ vs. $0.1347$												
2.249	2.053	0.1253	0.2312	5.166(-2)	1.895(-5)	3.502(-5)	3.236(-5)	0.9503	0.9576	-1.579(-3)	0.8813	
								0.9675	0.9727	-9.161(-4)	0.9207	
2.024	1.833	0.1448	0.2310	5.011(-2)	1.339(-5)	2.445(-5)	2.196(-5)	0.9274	0.9364	-2.956(-3)	0.8192	
								0.9533	0.9594	-1.667(-3)	0.8812	
1.934	1.740	0.1542	0.2309	4.951(-2)	2.925(-5)	4.763(-5)	3.735(-5)	0.9129	0.9231	-3.985(-3)	0.7790	
								0.9445	0.9514	-2.218(-3)	0.8570	
1.798	1.591	0.1702	0.2307	4.863(-2)	2.434(-5)	3.878(-5)	2.804(-5)	0.8797	0.8927	-6.541(-3)	0.6784	
								0.9261	0.9344	-3.513(-3)	0.8038	
1.753	1.535	0.1762	0.2307	4.835(-2)	2.135(-5)	3.350(-5)	2.248(-5)	0.8614	0.8761	-7.923(-3)	0.6138	
								0.9175	0.9265	-4.165(-3)	0.7783	
1.708	1.467	0.1826	0.2306	4.808(-2)	8.588(-7)	1.681(-5)	4.205(-7)	0.8290	0.8463	-1.042(-2)	0.4858	
								0.9068	0.9167	-5.008(-3)	0.7446	
1.694	1.443	0.1845	0.2306	4.800(-2)	3.132(-5)	2.533(-5)	4.673(-5)	0.8158	0.8340	-1.178(-2)	0.4422	
								0.9028	0.9131	-5.317(-3)	0.7318	

TABLE IX: Same as Table I but for  $\gamma = 1.8$ .

Identical mass stars, Synchronized case, $\gamma = 1.8$											
$\bar{d}_G$	$\bar{d}$	$\bar{\Omega}$	$\bar{M}$	$\bar{J}$	$ VE(M) $	$ VE(GB) $	$ VE(FUS) $	$a_2/a_1$	$a_3/a_1$	$\delta e_c$	$\chi$
$M/R = 0.08$ vs $0.08$ , $\bar{M}_B = 0.1485$ vs. $0.1485$											
7.747	2.340	0.02361	0.2852	0.1200	3.257(-6)	4.951(-6)	4.521(-6)	0.9771	0.9657	-1.777(-2)	0.9005
6.887	2.058	0.02800	0.2850	0.1155	2.891(-6)	4.363(-6)	3.941(-6)	0.9668	0.9499	-2.546(-2)	0.8546
6.026	1.763	0.03396	0.2849	0.1112	2.427(-6)	3.637(-6)	3.258(-6)	0.9475	0.9218	-3.873(-2)	0.7729
5.596	1.605	0.03779	0.2848	0.1092	2.044(-6)	3.034(-6)	2.689(-6)	0.9305	0.8985	-4.931(-2)	0.7047
5.165	1.434	0.04243	0.2848	0.1074	3.124(-6)	5.190(-6)	4.906(-6)	0.9026	0.8625	-6.482(-2)	0.5977
4.907	1.316	0.04571	0.2847	0.1066	2.566(-6)	3.873(-6)	3.543(-6)	0.8743	0.8285	-7.806(-2)	0.4951
4.820	1.271	0.04692	0.2847	0.1064	7.892(-6)	9.143(-6)	7.958(-6)	0.8604	0.8128	-8.351(-2)	0.4476
4.734	1.222	0.04818	0.2847	0.1062	1.199(-5)	1.547(-5)	1.478(-5)	0.8432	0.7937	-8.954(-2)	0.3890
$M/R = 0.10$ vs $0.10$ , $\bar{M}_B = 0.1725$ vs. $0.1725$											
6.887	2.319	0.02980	0.3281	0.1432	6.430(-6)	1.044(-5)	9.675(-6)	0.9768	0.9649	-2.239(-2)	0.8962
6.026	2.004	0.03608	0.3279	0.1376	5.553(-6)	8.969(-6)	8.212(-6)	0.9646	0.9459	-3.351(-2)	0.8404
5.596	1.840	0.04010	0.3278	0.1349	4.987(-6)	8.040(-6)	7.310(-6)	0.9544	0.9309	-4.212(-2)	0.7959
5.166	1.668	0.04494	0.3277	0.1323	4.330(-6)	7.046(-6)	6.344(-6)	0.9390	0.9089	-5.424(-2)	0.7311
4.908	1.559	0.04834	0.3277	0.1310	9.463(-6)	1.178(-5)	9.255(-6)	0.9253	0.8903	-6.412(-2)	0.6760
4.563	1.401	0.05362	0.3276	0.1294	1.203(-5)	1.661(-5)	1.410(-5)	0.8970	0.8541	-8.209(-2)	0.5678
4.391	1.311	0.05665	0.3275	0.1288	1.290(-5)	1.597(-5)	1.336(-5)	0.8743	0.8269	-9.420(-2)	0.4855
4.305	1.260	0.05828	0.3275	0.1286	1.476(-5)	2.046(-5)	1.787(-5)	0.8586	0.8090	-1.013(-1)	0.4309
$M/R = 0.12$ vs $0.12$ , $\bar{M}_B = 0.1920$ vs. $0.1920$											
6.887	2.607	0.03112	0.3622	0.1666	1.307(-5)	2.246(-5)	2.123(-5)	0.9835	0.9753	-2.125(-2)	0.9255
6.026	2.264	0.03764	0.3620	0.1598	1.153(-5)	1.970(-5)	1.841(-5)	0.9755	0.9623	-3.144(-2)	0.8865
5.166	1.907	0.04679	0.3617	0.1533	9.487(-6)	1.618(-5)	1.490(-5)	0.9597	0.9377	-4.980(-2)	0.8129
4.736	1.718	0.05287	0.3616	0.1503	8.299(-6)	1.421(-5)	1.296(-5)	0.9451	0.9162	-6.503(-2)	0.7487
4.306	1.514	0.06043	0.3614	0.1478	1.520(-5)	2.794(-5)	2.682(-5)	0.9198	0.8813	-8.808(-2)	0.6444
4.047	1.375	0.06589	0.3614	0.1466	2.016(-5)	3.009(-5)	2.594(-5)	0.8928	0.8471	-1.084(-1)	0.5414
3.961	1.324	0.06791	0.3613	0.1464	2.084(-5)	3.036(-5)	2.618(-5)	0.8797	0.8314	-1.169(-1)	0.4939
3.875	1.268	0.07004	0.3613	0.1461	2.752(-5)	4.055(-5)	3.707(-5)	0.8630	0.8120	-1.262(-1)	0.4351
$M/R = 0.14$ vs $0.14$ , $\bar{M}_B = 0.2065$ vs. $0.2065$											
6.456	2.748	0.03511	0.3868	0.1803	2.378(-5)	4.247(-5)	4.065(-5)	0.9860	0.9791	-2.779(-2)	0.9353
5.165	2.168	0.04808	0.3863	0.1690	1.918(-5)	3.423(-5)	3.209(-5)	0.9728	0.9572	-5.268(-2)	0.8686
4.305	1.754	0.06196	0.3860	0.1622	2.654(-5)	3.947(-5)	3.317(-5)	0.9493	0.9209	-8.992(-2)	0.7588
3.875	1.523	0.07163	0.3858	0.1595	2.584(-5)	3.656(-5)	2.994(-5)	0.9225	0.8832	-1.238(-1)	0.6452
3.703	1.419	0.07625	0.3857	0.1587	3.486(-5)	5.796(-5)	5.063(-5)	0.9042	0.8592	-1.428(-1)	0.5729
3.617	1.363	0.07876	0.3857	0.1584	3.603(-5)	5.962(-5)	5.219(-5)	0.8915	0.8436	-1.541(-1)	0.5259
3.531	1.302	0.08141	0.3857	0.1582	4.031(-5)	6.668(-5)	5.910(-5)	0.8753	0.8243	-1.668(-1)	0.4674
3.488	1.269	0.08280	0.3857	0.1581	5.067(-5)	8.384(-5)	7.517(-5)	0.8653	0.8127	-1.735(-1)	0.4325

TABLE X: Same as Table IX but for different mass binary systems. The prime denotes the values for the more massive star.

Different mass stars, Synchronized case, $\gamma = 1.8$											
$\bar{d}_G$	$\bar{d}$	$\bar{\Omega}$	$\bar{M}$	$\bar{J}$	$ VE(M) $	$ VE(GB) $	$ VE(FUS) $	$a_2/a_1$	$a_3/a_1$	$\delta e_c$	$\chi$
								$a'_2/a'_1$	$a'_3/a'_1$	$\delta e'_c$	$\chi'$
$M/R = 0.08$ vs $0.10$ , $\bar{M}_B = 0.1485$ vs. $0.1725$											
7.747	2.473	0.02440	0.3067	0.1335	5.001(-6)	7.956(-6)	7.382(-6)	0.9734	0.9617	-1.912(-2)	0.8890
								0.9860	0.9781	-1.478(-2)	0.9354
6.887	2.178	0.02892	0.3066	0.1285	4.532(-6)	7.170(-6)	6.587(-6)	0.9614	0.9440	-2.745(-2)	0.8377
								0.9801	0.9683	-2.097(-2)	0.9064
6.457	2.027	0.03174	0.3065	0.1259	4.226(-6)	6.671(-6)	6.095(-6)	0.9521	0.9307	-3.360(-2)	0.7990
								0.9756	0.9610	-2.545(-2)	0.8849
6.026	1.872	0.03505	0.3064	0.1235	3.877(-6)	6.127(-6)	5.562(-6)	0.9388	0.9124	-4.190(-2)	0.7457
								0.9695	0.9513	-3.136(-2)	0.8561
5.596	1.709	0.03898	0.3063	0.1212	3.464(-6)	5.487(-6)	4.950(-6)	0.9188	0.8858	-5.353(-2)	0.6682
								0.9607	0.9377	-3.937(-2)	0.8161
5.166	1.533	0.04373	0.3063	0.1191	3.302(-6)	5.186(-6)	4.666(-6)	0.8850	0.8439	-7.073(-2)	0.5442
								0.9474	0.9180	-5.064(-2)	0.7576
4.907	1.412	0.04708	0.3062	0.1181	1.115(-5)	1.408(-5)	1.234(-5)	0.8485	0.8021	-8.565(-2)	0.4191
								0.9355	0.9012	-5.985(-2)	0.7077
$M/R = 0.10$ vs $0.12$ , $\bar{M}_B = 0.1725$ vs. $0.1920$											
6.887	2.454	0.03047	0.3452	0.1543	9.525(-6)	1.601(-5)	1.504(-5)	0.9742	0.9621	-2.353(-2)	0.8881
								0.9852	0.9770	-2.031(-2)	0.9306
6.026	2.124	0.03687	0.3450	0.1482	8.344(-6)	1.394(-5)	1.295(-5)	0.9606	0.9417	-3.526(-2)	0.8279
								0.9780	0.9649	-3.005(-2)	0.8943
5.166	1.777	0.04589	0.3447	0.1423	6.858(-6)	1.155(-5)	1.056(-5)	0.9321	0.9015	-5.722(-2)	0.7095
								0.9637	0.9420	-4.757(-2)	0.8257
4.736	1.587	0.05189	0.3446	0.1398	6.736(-6)	1.128(-5)	1.016(-5)	0.9030	0.8636	-7.636(-2)	0.5973
								0.9505	0.9220	-6.204(-2)	0.7658
4.563	1.504	0.05469	0.3446	0.1389	1.792(-5)	2.685(-5)	2.361(-5)	0.8844	0.8408	-8.701(-2)	0.5296
								0.9429	0.9110	-6.981(-2)	0.7329
4.477	1.460	0.05618	0.3445	0.1385	1.819(-5)	2.616(-5)	2.282(-5)	0.8724	0.8267	-9.316(-2)	0.4873
								0.9384	0.9046	-7.415(-2)	0.7137
4.391	1.414	0.05775	0.3445	0.1381	2.022(-5)	2.732(-5)	2.379(-5)	0.8577	0.8099	-9.998(-2)	0.4366
								0.9332	0.8974	-7.888(-2)	0.6922
$M/R = 0.12$ vs $0.14$ , $\bar{M}_B = 0.1920$ vs. $0.2065$											
5.596	2.217	0.04239	0.3742	0.1643	1.547(-5)	2.693(-5)	2.543(-5)	0.9668	0.9498	-4.044(-2)	0.8488
								0.9803	0.9685	-4.070(-2)	0.9029
5.166	2.028	0.04744	0.3740	0.1609	1.408(-5)	2.449(-5)	2.298(-5)	0.9568	0.9346	-5.145(-2)	0.8035
								0.9747	0.9592	-5.124(-2)	0.8746
4.736	1.832	0.05359	0.3739	0.1576	1.263(-5)	2.166(-5)	2.077(-5)	0.9411	0.9119	-6.719(-2)	0.7359
								0.9663	0.9456	-6.600(-2)	0.8333
4.305	1.622	0.06120	0.3737	0.1548	2.080(-5)	2.979(-5)	2.463(-5)	0.9137	0.8748	-9.125(-2)	0.6256
								0.9527	0.9245	-8.739(-2)	0.7696
4.047	1.483	0.06670	0.3736	0.1534	2.426(-5)	3.658(-5)	3.140(-5)	0.8843	0.8383	-1.124(-1)	0.5161
								0.9397	0.9055	-1.053(-1)	0.7123
3.961	1.432	0.06872	0.3736	0.1530	2.527(-5)	3.762(-5)	3.233(-5)	0.8700	0.8213	-1.211(-1)	0.4652
								0.9340	0.8975	-1.125(-1)	0.6880
3.875	1.378	0.07086	0.3736	0.1526	3.746(-5)	4.675(-5)	4.142(-5)	0.8518	0.8007	-1.300(-1)	0.4028
								0.9273	0.8883	-1.205(-1)	0.6601

TABLE XI: Same as Table IX but for irrotational binaries.

Identical mass stars, Irrotational case, $\gamma = 1.8$											
$\bar{d}_G$	$\bar{d}$	$\bar{\Omega}$	$\bar{M}$	$\bar{J}$	$ VE(M) $	$ VE(GB) $	$ VE(FUS) $	$a_2/a_1$	$a_3/a_1$	$\delta e_c$	$\chi$
$M/R = 0.08$ vs $0.08$ , $\bar{M}_B = 0.1485$ vs. $0.1485$											
7.746	2.369	0.02363	0.2851	0.1147	3.139(-6)	4.714(-6)	4.269(-6)	0.9772	0.9804	-3.530(-4)	0.9387
6.024	1.812	0.03401	0.2848	0.1033	2.178(-6)	3.112(-6)	2.689(-6)	0.9480	0.9527	-1.476(-3)	0.8488
5.593	1.663	0.03785	0.2847	0.1004	1.839(-6)	2.535(-6)	2.128(-6)	0.9317	0.9373	-2.346(-3)	0.7966
5.162	1.504	0.04251	0.2845	0.09736	7.196(-6)	9.673(-6)	8.089(-6)	0.9050	0.9122	-4.010(-3)	0.7077
4.989	1.433	0.04465	0.2845	0.09616	7.030(-6)	9.188(-6)	7.585(-6)	0.8887	0.8968	-5.091(-3)	0.6494
4.816	1.354	0.04699	0.2844	0.09497	7.099(-6)	9.516(-6)	7.831(-6)	0.8648	0.8745	-6.631(-3)	0.5585
4.730	1.306	0.04825	0.2844	0.09439	6.175(-6)	9.979(-6)	8.045(-6)	0.8468	0.8576	-7.741(-3)	0.4858
4.643	1.245	0.04959	0.2844	0.09384	5.887(-7)	1.112(-5)	7.910(-6)	0.8190	0.8315	-9.440(-3)	0.3770
$M/R = 0.10$ vs $0.10$ , $\bar{M}_B = 0.1725$ vs. $0.1725$											
6.885	2.353	0.02983	0.3280	0.1365	6.157(-6)	9.913(-6)	9.110(-6)	0.9769	0.9806	-4.665(-4)	0.9372
5.163	1.730	0.04504	0.3275	0.1221	3.685(-6)	5.585(-6)	4.817(-6)	0.9401	0.9457	-2.309(-3)	0.8202
4.732	1.557	0.05100	0.3273	0.1183	3.314(-6)	4.566(-6)	3.868(-6)	0.9155	0.9225	-3.970(-3)	0.7353
4.559	1.483	0.05377	0.3272	0.1168	1.302(-5)	1.906(-5)	1.611(-5)	0.9004	0.9085	-5.156(-3)	0.6850
4.387	1.400	0.05682	0.3271	0.1153	1.205(-5)	1.747(-5)	1.439(-5)	0.8787	0.8881	-6.775(-3)	0.6030
4.300	1.352	0.05846	0.3271	0.1146	1.163(-5)	1.773(-5)	1.438(-5)	0.8626	0.8730	-7.880(-3)	0.5375
4.257	1.324	0.05931	0.3271	0.1142	1.048(-5)	1.804(-5)	1.426(-5)	0.8516	0.8628	-8.589(-3)	0.4921
4.213	1.291	0.06019	0.3271	0.1139	3.464(-6)	1.495(-5)	9.870(-6)	0.8371	0.8492	-9.611(-3)	0.4333
$M/R = 0.12$ vs $0.12$ , $\bar{M}_B = 0.1920$ vs. $0.1920$											
6.885	2.640	0.03115	0.3621	0.1600	1.266(-5)	2.172(-5)	2.045(-5)	0.9837	0.9874	-3.748(-4)	0.9574
5.163	1.965	0.04691	0.3615	0.1434	8.636(-6)	1.438(-5)	1.300(-5)	0.9604	0.9654	-1.553(-3)	0.8831
4.733	1.787	0.05303	0.3613	0.1390	7.042(-6)	1.150(-5)	1.015(-5)	0.9464	0.9522	-2.537(-3)	0.8373
4.302	1.599	0.06064	0.3610	0.1346	5.564(-6)	8.300(-6)	7.114(-6)	0.9227	0.9297	-4.481(-3)	0.7542
4.043	1.475	0.06617	0.3608	0.1320	2.167(-5)	3.418(-5)	2.909(-5)	0.8983	0.9069	-6.804(-3)	0.6687
3.870	1.375	0.07034	0.3607	0.1303	1.597(-5)	2.778(-5)	2.177(-5)	0.8685	0.8790	-9.350(-3)	0.5475
3.827	1.342	0.07146	0.3607	0.1298	1.084(-5)	2.310(-5)	1.594(-5)	0.8555	0.8669	-1.028(-2)	0.4923
3.783	1.302	0.07260	0.3607	0.1294	1.727(-5)	4.221(-7)	1.228(-5)	0.8366	0.8495	-1.204(-2)	0.4192
$M/R = 0.14$ vs $0.14$ , $\bar{M}_B = 0.2065$ vs. $0.2065$											
6.025	2.602	0.03877	0.3865	0.1691	2.183(-5)	3.889(-5)	3.688(-5)	0.9833	0.9874	-6.324(-4)	0.9554
4.302	1.840	0.06217	0.3856	0.1501	1.315(-5)	2.284(-5)	2.060(-5)	0.9518	0.9576	-3.291(-3)	0.8510
3.872	1.633	0.07197	0.3853	0.1452	2.359(-5)	3.504(-5)	2.722(-5)	0.9282	0.9354	-6.118(-3)	0.7701
3.699	1.543	0.07664	0.3851	0.1433	2.193(-5)	3.218(-5)	2.409(-5)	0.9128	0.9210	-8.110(-3)	0.7146
3.613	1.495	0.07919	0.3850	0.1423	3.590(-5)	6.044(-5)	5.216(-5)	0.9025	0.9113	-9.426(-3)	0.6751
3.527	1.441	0.08186	0.3850	0.1414	3.051(-5)	5.176(-5)	4.295(-5)	0.8884	0.8981	-1.111(-2)	0.6173
3.440	1.372	0.08469	0.3849	0.1404	2.422(-6)	1.779(-5)	4.755(-5)	0.8629	0.8744	-1.382(-2)	0.5056
3.414	1.344	0.08555	0.3849	0.1401	3.859(-5)	2.961(-5)	4.862(-5)	0.8498	0.8624	-1.561(-2)	0.4548

TABLE XII: Same as Table XI but for different mass binary systems. The prime denotes the values of the more massive star.

Different mass stars, Irrotational case, $\gamma = 1.8$												
$\bar{d}_G$	$\bar{d}$	$\bar{\Omega}$	$\bar{M}$	$\bar{J}$	$ VE(M) $	$ VE(GB) $	$ VE(FUS) $	$a_2/a_1$	$a_3/a_1$	$\delta e_c$	$\chi$	
								$a'_2/a'_1$	$a'_3/a'_1$	$\delta e'_c$	$\chi'$	
$M/R = 0.08$ vs $0.10$ , $\bar{M}_B = 0.1485$ vs. $0.1725$												
6.885	2.215	0.02895	0.3065	0.1219	4.305(-6)	6.716(-6)	6.103(-6)	0.9616	0.9662	-9.151(-4)	0.8936	
								0.9802	0.9832	-3.373(-4)	0.9453	
6.024	1.920	0.03510	0.3063	0.1155	3.552(-6)	5.429(-6)	4.824(-6)	0.9395	0.9453	-1.994(-3)	0.8253	
								0.9697	0.9732	-6.930(-4)	0.9125	
5.593	1.766	0.03905	0.3062	0.1122	3.105(-6)	4.674(-6)	4.078(-6)	0.9202	0.9271	-3.162(-3)	0.7635	
								0.9611	0.9651	-1.058(-3)	0.8852	
5.162	1.601	0.04382	0.3060	0.1089	7.671(-6)	9.319(-6)	7.207(-6)	0.8878	0.8966	-5.419(-3)	0.6543	
								0.9482	0.9529	-1.730(-3)	0.8435	
4.903	1.489	0.04719	0.3059	0.1069	1.043(-5)	1.441(-5)	1.228(-5)	0.8520	0.8631	-7.873(-3)	0.5200	
								0.9370	0.9422	-2.395(-3)	0.8061	
4.817	1.444	0.04841	0.3059	0.1063	9.242(-6)	1.367(-5)	1.134(-5)	0.8315	0.8438	-9.215(-3)	0.4389	
								0.9323	0.9378	-2.694(-3)	0.7902	
4.774	1.418	0.04905	0.3059	0.1059	8.011(-6)	1.343(-5)	1.090(-5)	0.8176	0.8308	-1.009(-2)	0.3862	
								0.9296	0.9353	-2.863(-3)	0.7811	
$M/R = 0.10$ vs $0.12$ , $\bar{M}_B = 0.1725$ vs. $0.1920$												
6.024	2.169	0.03693	0.3448	0.1401	7.857(-6)	1.298(-5)	1.192(-5)	0.9609	0.9660	-1.175(-3)	0.8892	
								0.9782	0.9818	-5.580(-4)	0.9388	
5.163	1.838	0.04600	0.3445	0.1322	6.053(-6)	9.781(-6)	8.722(-6)	0.9333	0.9399	-2.852(-3)	0.8010	
								0.9643	0.9686	-1.246(-3)	0.8938	
4.732	1.661	0.05204	0.3443	0.1282	1.283(-5)	1.715(-5)	1.347(-5)	0.9055	0.9138	-4.959(-3)	0.7081	
								0.9516	0.9566	-2.071(-3)	0.8520	
4.474	1.544	0.05636	0.3442	0.1258	1.261(-5)	1.659(-5)	1.277(-5)	0.8764	0.8865	-7.252(-3)	0.6017	
								0.9403	0.9460	-2.903(-3)	0.8141	
4.387	1.501	0.05794	0.3441	0.1249	1.869(-5)	2.749(-5)	2.371(-5)	0.8614	0.8724	-8.269(-3)	0.5423	
								0.9356	0.9415	-3.263(-3)	0.7979	
4.301	1.451	0.05959	0.3441	0.1241	1.429(-5)	2.389(-5)	1.952(-5)	0.8386	0.8511	-9.973(-3)	0.4497	
								0.9301	0.9363	-3.730(-3)	0.7790	
4.257	1.421	0.06046	0.3440	0.1238	7.698(-6)	1.907(-5)	1.365(-5)	0.8218	0.8354	-1.128(-2)	0.3869	
								0.9270	0.9333	-3.992(-3)	0.7679	
$M/R = 0.12$ vs $0.14$ , $\bar{M}_B = 0.1920$ vs. $0.2065$												
6.025	2.445	0.03824	0.3742	0.1602	1.616(-5)	2.830(-5)	2.665(-5)	0.9739	0.9786	-8.166(-4)	0.9281	
								0.9845	0.9881	-5.401(-4)	0.9581	
5.163	2.087	0.04756	0.3738	0.1513	1.334(-5)	2.314(-5)	2.141(-5)	0.9575	0.9631	-1.799(-3)	0.8753	
								0.9754	0.9796	-1.121(-3)	0.9284	
4.302	1.709	0.06143	0.3733	0.1421	2.074(-5)	3.023(-5)	2.431(-5)	0.9170	0.9249	-5.224(-3)	0.7401	
								0.9548	0.9602	-2.910(-3)	0.8598	
4.043	1.583	0.06698	0.3731	0.1394	1.937(-5)	2.788(-5)	2.166(-5)	0.8900	0.8995	-7.801(-3)	0.6417	
								0.9433	0.9493	-4.155(-3)	0.8205	
3.957	1.537	0.06902	0.3731	0.1384	1.873(-5)	2.699(-5)	2.066(-5)	0.8759	0.8863	-9.045(-3)	0.5853	
								0.9384	0.9447	-4.742(-3)	0.8034	
3.871	1.484	0.07118	0.3730	0.1375	1.973(-5)	3.222(-5)	2.534(-5)	0.8540	0.8660	-1.078(-2)	0.4933	
								0.9327	0.9393	-5.420(-3)	0.7832	
3.801	1.430	0.07298	0.3730	0.1368	6.762(-6)	6.274(-6)	4.582(-6)	0.8234	0.8377	-1.374(-2)	0.3815	
								0.9272	0.9341	-6.047(-3)	0.7634	